



**HAL**  
open science

# Summertime dust storms over the Arabian Peninsula and impacts on radiation, circulation, cloud development and rain

Diana Francis, Jean-Pierre Chaboureau, Narendra Nelli, Juan Cuesta, Noor Alshamsi, Marouane Temimi, Olivier Pauluis, Lulin Xue

► **To cite this version:**

Diana Francis, Jean-Pierre Chaboureau, Narendra Nelli, Juan Cuesta, Noor Alshamsi, et al.. Summertime dust storms over the Arabian Peninsula and impacts on radiation, circulation, cloud development and rain. *Atmospheric Research*, 2021, 250, pp.105364. 10.1016/j.atmosres.2020.105364. hal-04253270

**HAL Id: hal-04253270**

<https://hal.science/hal-04253270v1>

Submitted on 22 Oct 2023

**HAL** is a multi-disciplinary open access archive for the deposit and dissemination of scientific research documents, whether they are published or not. The documents may come from teaching and research institutions in France or abroad, or from public or private research centers.

L'archive ouverte pluridisciplinaire **HAL**, est destinée au dépôt et à la diffusion de documents scientifiques de niveau recherche, publiés ou non, émanant des établissements d'enseignement et de recherche français ou étrangers, des laboratoires publics ou privés.



Distributed under a Creative Commons Attribution 4.0 International License



## Summertime dust storms over the Arabian Peninsula and impacts on radiation, circulation, cloud development and rain

Diana Francis<sup>a,\*</sup>, Jean-Pierre Chaboureau<sup>b</sup>, Narendra Nelli<sup>a</sup>, Juan Cuesta<sup>c</sup>, Noor Alshamsi<sup>d</sup>, Marouane Temimi<sup>e</sup>, Olivier Pauluis<sup>d</sup>, Lulin Xue<sup>f</sup>

<sup>a</sup> Khalifa University of Science and Technology, P. O. Box 54224, Abu Dhabi, United Arab Emirates

<sup>b</sup> Laboratoire d'Aérodynamique, Université de Toulouse, CNRS, UPS, Toulouse, France

<sup>c</sup> Laboratoire Interuniversitaire des systèmes atmosphériques, CNRS and Université Paris-Est Créteil Val de Marne, France

<sup>d</sup> New York University Abu Dhabi, P.O. Box 129188, Abu Dhabi, United Arab Emirates

<sup>e</sup> Department of Civil, Environmental, Ocean Engineering (CEOE), Stevens Institute of Technology, Hoboken, NJ 07030, USA

<sup>f</sup> National Center for Atmospheric Research - NCAR, Boulder, CO, USA

### ARTICLE INFO

#### Keywords:

Dust aerosols  
Radiative forcing  
Cyclogenesis  
Convective clouds  
Southwest Asia  
AEROIASI  
SEVIRI  
CALIPSO  
Meso-NH

### ABSTRACT

This study investigates the underlying atmospheric dynamics associated with intense dust storms in summer 2018 over the Arabian Peninsula (AP); a major dust source at global scale. It reports, for the first time, on the formation of cyclone over the Empty Quarter Desert as important mechanism for intense dust storms over this source region. The dust direct and semi-direct radiative forcings are observed, for the first time over this source region, using high-resolution in-situ and CERES-SYN satellite observational data. The three-dimensional structure and evolution of the dust storms are inferred from state-of-the-art satellite products such as SEVIRI, AEROIASI and CALIPSO. The dynamics and thermodynamics of the boundary layer during this event are thoroughly analyzed using ERA5 reanalysis and ground based observations. We found that a large dust storm by Shamal winds led up, through radiative forcing, to cyclone development over the Empty Quarter Desert, subsequent dust emissions, development of convective clouds and rain. The cyclogenesis over this region initiated a second intense dust storm which developed and impacted the AP for 3 consecutive days. The uplifted dust by the cyclone reached 5 km in altitude and altered the radiative budget at the surface, inducing both significant warming during night and cooling during day. The dust load uplifted by the cyclone was estimated by the mesoscale model Meso-NH to be in the order of 20 Tg, and the associated aerosol optical depth was higher than 3. The model simulates reasonably the radiative impact of the dust in the shortwave but highly underestimated its impact in the LW. Our study stresses the importance of the dust radiative forcing in the longwave and that it should be accurately accounted for in models to properly represent the impact of dust on the Earth system especially near source areas. Missing the warming effect of dust aerosols would impact both the weather and air quality forecast, and the regional climate projections.

### 1. Introduction

Despite being emitted from relatively limited areas around the globe, atmospheric dust is recognized as an important component of the Earth's climate system (e.g., IPCC, 2013), contributing largely to the global population of natural aerosols (Prospero et al., 2002; Tanaka and Chiba, 2006). Atmospheric dust particles can serve as cloud condensation nuclei (e.g., Karydis et al., 2011) and ice nucleating particles (e.g., Boose et al., 2016), thereby altering cloud development, properties and associated precipitation. Furthermore, mineral dust aerosols are known

to strongly influence the radiative budget due to their significant scattering, absorbing and re-emitting properties (Haywood et al., 2005; Sokolik and Toon, 1996; Dubovik et al., 2006; Prakash et al., 2015). By virtue of their distinctive optical properties, mineral dust aerosols scatter and absorb shortwave (SW) and absorb and re-emit longwave (LW) radiation (e.g., Tegen and Lacis, 1996; Kinne et al., 2003; Dubovik et al., 2006), modifying therefore atmospheric thermodynamics, regional atmospheric circulations and the Earth's energy budget (e.g., Slingo et al., 2006; Sokolik and Toon, 1996; Heald et al., 2014). By modifying the radiative forcing, dust aerosols affect local climatic

\* Corresponding author.

E-mail address: [diana.francis@ku.ac.ae](mailto:diana.francis@ku.ac.ae) (D. Francis).

<https://doi.org/10.1016/j.atmosres.2020.105364>

Received 2 July 2020; Received in revised form 7 October 2020; Accepted 10 November 2020

Available online 12 November 2020

0169-8095/© 2020 The Authors. Published by Elsevier B.V. This is an open access article under the CC BY license (<http://creativecommons.org/licenses/by/4.0/>).

parameters such as temperature, winds and precipitation (Sharma et al., 2012; Rap et al., 2013; Liu et al., 2014; Chen et al., 2017).

For instance, dust aerosols were found to increase the mass of water in the atmospheric column over the Arabian Peninsula (AP) by 0.5 g per kg of dry air as daily average via interactions with radiation and subsequent impact on the circulation (Spyrou, 2018). Through this process dust enhances its own greenhouse effect, further increasing the surface temperature and humidity (Spyrou, 2018). Over the Sahara, dust aerosols were found to be of similar importance as water vapor in driving variability in the top-of-atmosphere radiation budget (Banks et al., 2014). The induced column-integrated heating was found to be more than  $7 \text{ Wm}^{-2}$  per standard deviation of dust aerosol optical depth, almost entirely in the longwave as the effects of shortwave absorption with respect to surface albedo largely balance (Alamirew et al., 2018). Moreover, via the direct effect on radiation, dust can increase the concentration of polluted aerosols by changing the regional circulation patterns and enhancing air stagnation in some cases (Yang et al., 2017). Additionally, dust over source areas directly heats the PBL by  $0.6 \text{ Kday}^{-1}$  (Alamirew et al., 2018) and alter the daytime and nighttime surface heating and low-level temperature profiles (Saleeby et al., 2019), which has implications on the development of mesoscale weather features such as convection and sea breeze, whose circulations are driven or initiated by horizontal heterogeneities in local-scale thermal contrasts (e.g., Eager et al., 2008; Crosman and Horel, 2010; Ge et al., 2014).

Through the absorption and scattering of solar radiation, dust aerosols reduce the amount of energy reaching the surface (e.g., Kosmopoulos et al., 2017; Jia et al., 2018), which can lead to reduced surface heating and thus reduced latent and sensible heat fluxes (Wang et al., 2004; Prakash et al., 2015; Kaskaoutis et al., 2019a). At the same time, dust absorption of both longwave and shortwave radiation can contribute to localized heating by directly warming the dust-laden atmospheric layer (e.g., Weston et al., 2020) and enhance the greenhouse effect by emitting longwave radiation towards the surface (Heinold et al., 2008). Within the dust layer, a cooling tendency may also exist due to longwave emission, with a warming tendency adjacent to it (e.g., Wang et al., 2013a, 2013b). In all cases, the intensity of the radiative impact of dust in both SW and LW depends strongly on the location of the dust layer in altitude (e.g., Saleeby et al., 2019) and whether it's over water, vegetated areas or desert lands (e.g., Wang et al., 2013a).

Given the sporadic nature of dust storms, the complex balance between their absorption, scattering and emission of radiation as well as the heterogeneity in their impact on radiation and feedback on climate, it has been difficult to assess their net impact on the regional and global climate; which introduces one of the main sources of uncertainties in future climate projections (e.g., Myhre et al., 2013; Boucher et al., 2013; IPCC, 2013). For instance, global climate models underestimate the warming effect of dust by more than  $0.15 \text{ Wm}^{-2}$  as they underestimate by four times the amount of coarse dust in the atmosphere (Adebiyi and Kok, 2020). Accounting for this missing coarse dust adds a warming effect and implies that dust net impact warms the climate system (Adebiyi and Kok, 2020), contrary to what has been thought before where mineral dust was believed to induce a net cooling and counteracting the warming effect of greenhouse gases (e.g., IPCC, 2013). This becomes even more significant near major dust source regions, where the coarse dust is abundant (e.g., Francis et al., 2019c), the heating effect of episodic synoptic and mesoscale dust events can reach  $6 \text{ K day}^{-1}$  (Alamirew et al., 2018), and the direct dust–climate feedback is believed to be enhanced by over an order of magnitude (e.g., Kok et al., 2018).

An essential phase in the dust cycle is the emission and transport of dust aerosols from source areas. This phase is mainly controlled by atmospheric processes which determine the time of the occurrence of the dust storm, its intensity, its duration, mixing, accumulation and transport (e.g., Schepanski, 2018). Therefore, it is crucial to identify the mechanism driving dust emissions and transport from source regions in order to be able to represent them correctly in climate models which in turn will help to account accurately for the dust impacts.

Located in the dust belt, the Arabian Peninsula (AP) is one of the major dust sources at global scale (e.g., Prospero et al., 2002) active year round with a peak in dust activity in summer (Mashat et al., 2008; Hermida et al., 2018). Frequent dust outbreaks (e.g. Yu et al., 2015) and 15 to 20 major dust storms per year occur over the AP (Prakash et al., 2015) and impact all aspects of human activity (e.g., Goudie, 2014; Middleton and Kang, 2017), marine ecosystems (Guieu et al., 2019) and the climate system (e.g., Jin et al., 2015; Notaro et al., 2015). Even though the Arabian Peninsula contributes substantially to the total lofted dust load in the Northern Hemisphere (Tanaka and Chiba, 2006), few studies have focused on the radiative impact of dust over this region and were either based on modelling estimate (e.g., Prakash et al., 2015) or focused on a limited area (e.g., Saeed et al., 2014). As such, the mechanisms involved in summertime dust emissions over the AP are not completely understood and the effect of dust loads on the circulation over this region, via interactions with radiation and cloud-precipitation processes, have not been examined so far.

Over the AP, Shamal winds; the northerly semi-permanent winds resulting from the east-west pressure gradient between the subtropical low-pressure system over southwest Asia and the subtropical high-pressure system over north Africa (e.g., Ali, 1994; Krishnamurti et al., 2013), are thought to be the main meteorological driver for dust emissions year round, with a peak in summer when the pressure gradient is the strongest (Yu et al., 2016; Bou Karam Francis et al., 2017). On the diurnal scale, the peak in dust activity is noticed during morning hours due to the downward mixing of high-momentum from the nocturnal low level jet (LLJ) by intense turbulent mixing after solar heating commences each day at sunrise (Giannakopoulou and Toumi, 2012; Todd et al., 2008; Bou Karam Francis et al., 2017). The compaction of the east–west pressure gradient between the Zagros Mountains in Iran and the Njaf Plateau in Saudi Arabia, further intensifies the Shamal-related LLJ winds while restricting them to the eastern side of the AP (e.g., Rao et al., 2001), which results in high Shamal-related dust activity over the eastern and central parts of the AP.

Additional dust emissions can occur during winter associated with the intrusion of cold fronts from mid-latitudes (e.g., Kaskaoutis et al., 2019b). Disturbances from mid-latitudes such as cut-off lows and cut-off highs were also found to cause large dust storms when they occur over the northern parts of the AP where they promote the formation of dry cyclones and density currents over the Middle East (Francis et al., 2019c).

However, the peak in dust emissions over the southern parts of the AP during summer indicates the existing of still-unknown but important mechanisms for dust emissions. Of particular relevance to this region; cyclogenesis, which has proven to be a major dust emission mechanism over other arid regions (e.g., Kaskaoutis et al., 2015; Saeedi and Khoshkhalagh, 2019), being capable of generating dramatic dust storms associated with heavy dust loads up to 250 tons per episode over the Middle East (Francis et al., 2019c) and 8 Tg over North Africa (Bou Karam et al., 2010; Fiedler et al., 2014; Francis et al., 2018, 2019a).

Despite their effective role in dust emission and transport over long distance, no attention has been given to dust activity associated with cyclogenesis over the AP, one of the major dust sources in the dust belt and where favorable synoptic conditions for cyclogenesis are a ubiquitous feature during summer (e.g., Notaro et al., 2015; Yu et al., 2015). In fact, the convergence between the northerly and the southerly winds during summer when the southerlies (e.g., Dumka et al., 2019), being embedded in the larger southerly monsoon flow, advance inland and promote the formation of cyclones along this interface (e.g., Bou Karam et al., 2009a; Rashki et al., 2019). For instance, this mechanism was found to operate over West Africa during the summer season with cyclogenesis occurring at low levels along the convergence zone over land between the southerlies and the northerlies (i.e., Bou Karam et al., 2008, 2009).

In this study, we report for the first time, the occurrence of cyclogenesis over the Empty Quarter Desert (Fig. 1) where these two flows

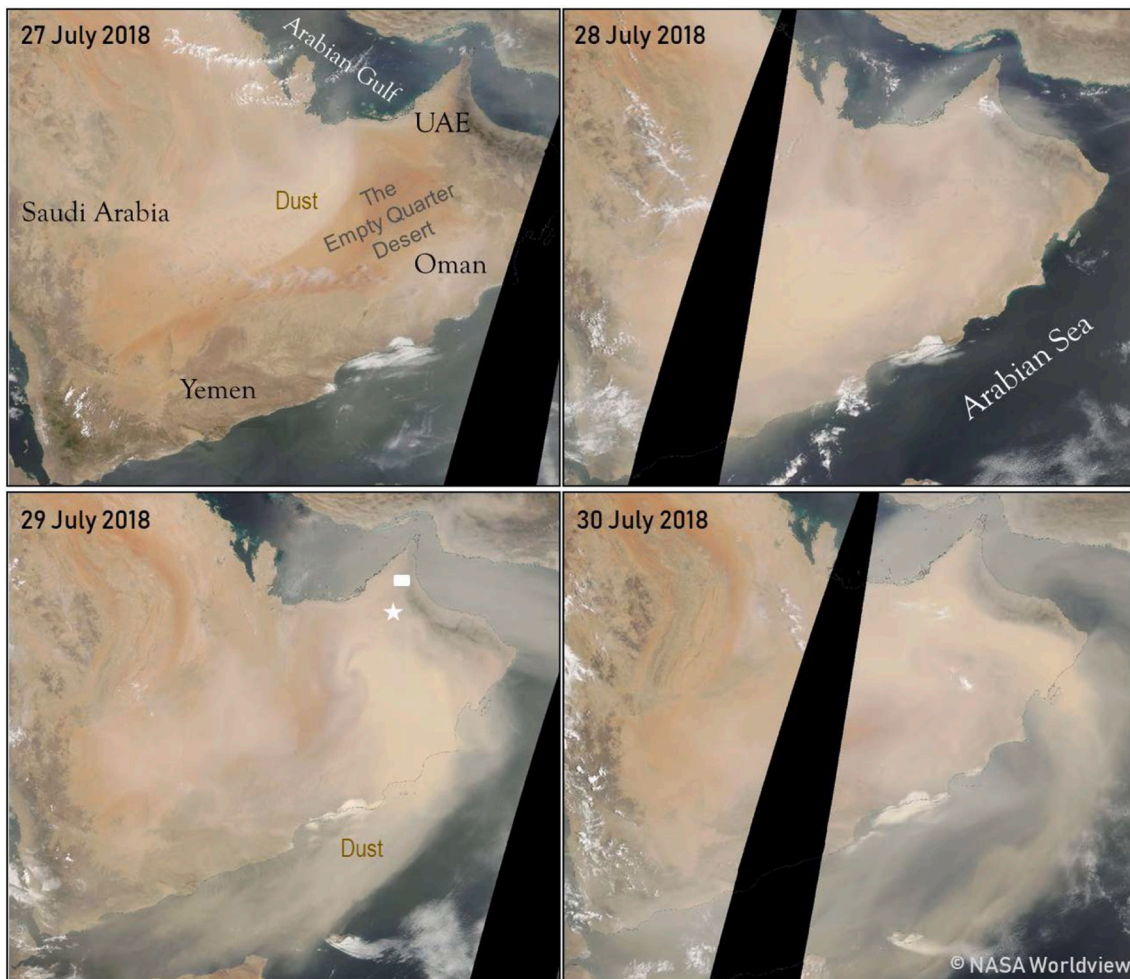


Fig. 1. MODIS satellite visible imagery showing the dust storm on 27–30 July 2018 over the Arabian Peninsula. The white star represents the location of Gasyoura automatic weather station in United Arab Emirates (UAE) and the white square represents the location of Al Ain station. Image credit: NASA Worldview.

converge during summer and we identify it as an important mechanism for dust activity over the southern AP.

The objective of this study is to (i) investigate the intense dust activity that occurred over the AP in July 2018, (ii) identify the underlying atmospheric dynamics and (iii) assess for the first time the radiative impact of dust on the atmospheric circulation and subsequently on cloud and rain development. The paper is organized as follows: Section 2 describes the data sets and the numerical model experiments used in this study. The results are detailed in Section 3 including the characteristics of the dust storms, the cyclone formation, and the associated dust emissions and convective clouds. Section 4 investigates the radiative impact of the cyclone-induced dust storm. Section 5 discusses the results of the numerical model simulations. Section 6 concludes the paper.

## 2. Data

### 2.1. Reanalysis data

To address the atmospheric circulation at regional scale during the dust storms and to investigate the atmospheric dynamics that triggered the cyclone formation, we use the European Center for Medium Weather Forecast (ECMWF) ERA 5 reanalysis (Hersbach et al., 2020) for their higher temporal and spatial resolution (hourly at approximately 31 km with 137 levels to 0.01 hPa). ERA5 was produced by the most recent model system with a more advanced data assimilation component compared to previous reanalysis data produced by ECMWF.

### 2.2. Satellite observations

Observations at high spatio-temporal resolution from the Spinning Enhanced Visible and Infrared Imager (SEVIRI) on board the Meteosat Second Generation (MSG-SEVIRI) geostationary satellite are used in this study in order to characterize qualitatively the dust activity over the Arabian Peninsula. The evolution of the dust storms is described using the SEVIRI images computed from a combination of three infrared channels, namely channel 10 (12  $\mu\text{m}$ ), channel 9 (10.8  $\mu\text{m}$ ) and channel 7 (8.7  $\mu\text{m}$ ). MSG-SEVIRI is located geostationary at 0°W over the equator and provides images of Southwest Asia on a 15 min temporal resolution. False-color images are created using an algorithm developed by EUMETSAT in which the red color represents the brightness temperature difference between the 12.0 and 10.8  $\mu\text{m}$  channels, green the difference between the 10.8 and 8.7  $\mu\text{m}$  channels and blue the 10.8  $\mu\text{m}$  channel (e.g., Banks et al., 2018). On these false-color composite images, clouds appear orange or brown with thick, high-level clouds in red-brown tones and thin high-level clouds appear very dark (nearly black). Dry land looks from pale blue (daytime) to pale green (nighttime). In the Desert Dust false-color imagery, dust appears pink or magenta with the clearest pink colors arising from high-altitude dust in dry atmospheres. However, the precise color is influenced by numerous environmental properties, such as the surface thermal emissivity and skin temperature, the atmospheric water vapor content, the quantity and height of dust in the atmosphere, and the infrared optical properties of the dust itself. The content of water vapor is found to be the major control on the apparent

color of dust, obscuring its presence when the moisture content is high or when the dust is near the surface below the atmospheric water vapor column (Banks et al., 2018). Dust close to the surface (altitude <1 km) is only likely to be detected when the atmosphere is particularly dry and when the surface is particularly hot. Note that the dust effect on brightness temperature differences depends on its altitude suggesting that these composite images may favor the dust which is elevated so that its radiating temperature differs significantly from the ground.

Furthermore, to observe the three-dimensional (3D) distribution of desert dust plumes (vertical and horizontal) we use the newly-developed retrieval: AEROIASI (Cuesta et al., 2015) version 2. This approach uses IASI hyperspectral observations (Clerbaux et al., 2009; provided by AERIS/ESPRI data center <https://iasi.aeris-data.fr>) to provide a 3D map of dust distribution for each overpass of IASI, both over land and ocean. AEROIASI gives also mean and top altitudes of dust layers together with the associated Aerosol Optical Depth (AOD) at 10  $\mu\text{m}$ . Detailed information on the AEROIASI retrieval of dust distribution can be found in Cuesta et al. (2015, 2020).

Furthermore, information about the vertical distribution of dust is provided from particle extinction coefficient profiles at 532 nm derived from CALIOP measurements of attenuated backscatter profiles (or reflectivity profiles at 532 nm). They are obtained from our own calculation (using level 1B version 3.30 data) as that by Cuesta et al. (2009), with a vertical resolution of 60 m and a horizontal resolution of roughly 12 km. We expect the uncertainty on the extinction coefficient and on the AOD to be on the order of 30% (and may be greater for AOD greater than 2), accounting for an uncertainty of 20% on both the backscatter-to-extinction ratio and the multiple scattering coefficients. It is worth noting that all the instruments/platforms are part of the A-Train except for MSG. The A-train orbit overpasses the Middle East twice a day, once during the daytime (between 0940 and 1000 UTC, Coordinated Universal Time) and once during the night-time (between 1130 and 0000 UTC), and has a revisit time period of the same orbit of 16 days (Stephens et al., 2002). The data is available through the ICARE Web portal (<http://www.icare.univ-lille1.fr>). Additionally, AODs from the Moderate Resolution Imaging Spectroradiometer (MODIS; Kaufman et al., 1997) collocated with the ground-based measurements of radiative fluxes were used to address the temporal evolution of AOD during the study period.

For surface (SFC) and top-of-atmosphere (TOA) radiative flux quantities, we use the satellite-derived Clouds and the Earth's Radiant Energy System Synoptic (CERES-SYN) version 3 data set (Wielicki et al., 1996). CERES-SYN provides hourly shortwave (SW) and longwave (LW) surface and TOA flux quantities over a  $1^\circ \times 1^\circ$  resolution grid in both clear-sky and all-sky conditions.

### 2.3. Ground-based observations

The hourly measurements of 2-m air temperature, relative humidity, winds, pressure and SW radiation fluxes at Gasyoura (the star on Fig. 1) are from an automated weather and radiometer station and are provided by the National Center for Meteorology (NCM) in the United Arab Emirates (UAE). The observations at Al Ain (the square on Fig. 1) are part of the NCM's UAE Rain Enhancement Program (UAEREP) global research initiative (<http://www.uaerep.ae/>). For more details about these observations, see Nelli et al. (2020).

### 2.4. Model simulations

The Meso-NH (version 5-3-0) atmospheric model (Lafore et al., 1998; Lac et al., 2018) was utilized to simulate the dust storms and their radiative impact. Meso-NH is a non-hydrostatic mesoscale model coupled with an on-line dust emission and transport module (Grini et al., 2006). Meso-NH model has been extensively validated over several arid regions against ground-based, airborne and satellite datasets (e.g., Mallet et al., 2009; Bou Karam et al., 2008, 2010, Bou Karam et al.,

2014; Chaboureau et al., 2011) and is very capable in simulating the atmospheric dynamics for dust mobilization, dust emission and transport pathways as several previous studies have shown (e.g., Todd et al., 2008; Bou Karam et al., 2009a, 2009b; Chaboureau et al., 2016; Francis et al., 2018, 2019a). In this study, the model was run during 6 days (from 26 July 2018 at 00:00 UTC to 1 August 2018 at 00:00 UTC) over the domain  $32^\circ - 62^\circ\text{E}$ ,  $12^\circ - 40^\circ\text{N}$ , using a horizontal grid of 12-km and 72 levels in the vertical (10 m – 28 km), 35 of which within the planetary boundary layer (i.e., below 2 km). The initial and boundary conditions were taken from the ECMWF operational analysis. The model run used a Rapid Radiative Transfer Model parameterization (Mlawer et al., 1997), a mixed-phase bulk microphysical scheme (Pinty and Jabouille, 1998), a turbulence parameterization (Cuxart et al., 2000), a convective mass-flux scheme (Bechtold et al., 2001) and a sub-grid cloud cover and condensate content scheme (Chaboureau and Bechtold, 2005). The dust scheme includes the Dust Entrainment and Deposition (DEAD) scheme (Zender et al., 2003) and the ORganic and Inorganic Log-normal Aerosols Model (ORILAM; Tulet et al., 2005), which parameterizes the transport, dry and wet deposition of dust as well as the dust interactions with SW and LW radiation. In this scheme, generation, transport and loss processes of dust are simulated by following the evolution of the number and mass of three log-normal modes of dust. Their initial size distribution is set with median diameters of 0.078, 0.64 and 5.0  $\mu\text{m}$  and standard deviations of 1.75, 1.76 and 1.70, respectively. The radiative properties of dust were obtained, in the shortwave spectrum, from the photometers deployed during the African Monsoon Multidisciplinary Analyses (AMMA) program while, in the longwave, the standard formulation of absorption and re-emission for aerosols from the ECMWF model was used (see Mallet et al., 2009, for more details). It is worth mentioning that the indirect effect of dust aerosols i.e., their interactions with clouds and with other types of aerosols is not accounted for in the simulations.

## 3. Characteristics of the dust storms in July 2018

### 3.1. Shamal-wind dust storm over Saudi Arabia on 26–27 July 2018

The period between 26 and 28 July 2018 was characterized by a ridging of the subtropical high over Libya (Fig. 2a). At the same time, a deep trough was present at low levels over Afghanistan and Pakistan and stretching towards the Arabian Gulf (Fig. 2a). This dipole in pressure at low levels resulted in a surge in the northwesterly winds over the Arabian Peninsula (Fig. 2a) known as Shamal winds (e.g., Bou Karam Francis et al., 2017). At 850 hPa, high wind speeds up to 20  $\text{m s}^{-1}$  blew over Iraq and Saudi Arabia (Fig. 2a), where major dust sources are present (Prospero et al., 2002). This, resulted in intense dust emissions and southward transport (Fig. 2b). SEVIRI false-color images showed an arc-shaped dense dust cloud covering most of the southern half of Saudi Arabia, encompassing more than 10 degrees in longitudes and 10 degrees in latitudes (Fig. 2b).

Significant increase in LW downwelling radiation at the surface was observed in the CERES-SYN measurements shown in Fig. 2c. Up to 100  $\text{W m}^{-2}$  instantaneous increase in LW fluxes occurred at the surface in the region underneath the dust cloud compared to the day before the dust storm. A clear footprint of the dust cloud was visible in the radiation measurements at the surface (Fig. 2c) and shifted southward (Fig. 2d) as the dust moved towards the southern coast of the Arabian Peninsula (AP). This warming effect induced by the dust increased the temperature gradient between land and the surroundings seas (i.e., the Arabian Gulf to the east of the AP and the Arabian Sea to the south) especially during night when colder temperatures are expected over land compared to surrounding seas. Skin temperatures over land at 9 pm local time were more than 7  $^\circ\text{C}$  warmer than temperatures over the Arabian Gulf and more than 12  $^\circ\text{C}$  warmer than surface temperatures over the Arabian Sea (Fig. 2e). The dust-induced temperature gradient between land and sea promoted sustained intrusions of moist air masses from the Arabian Gulf and the Arabian Sea towards the desert areas during the entire day on 27

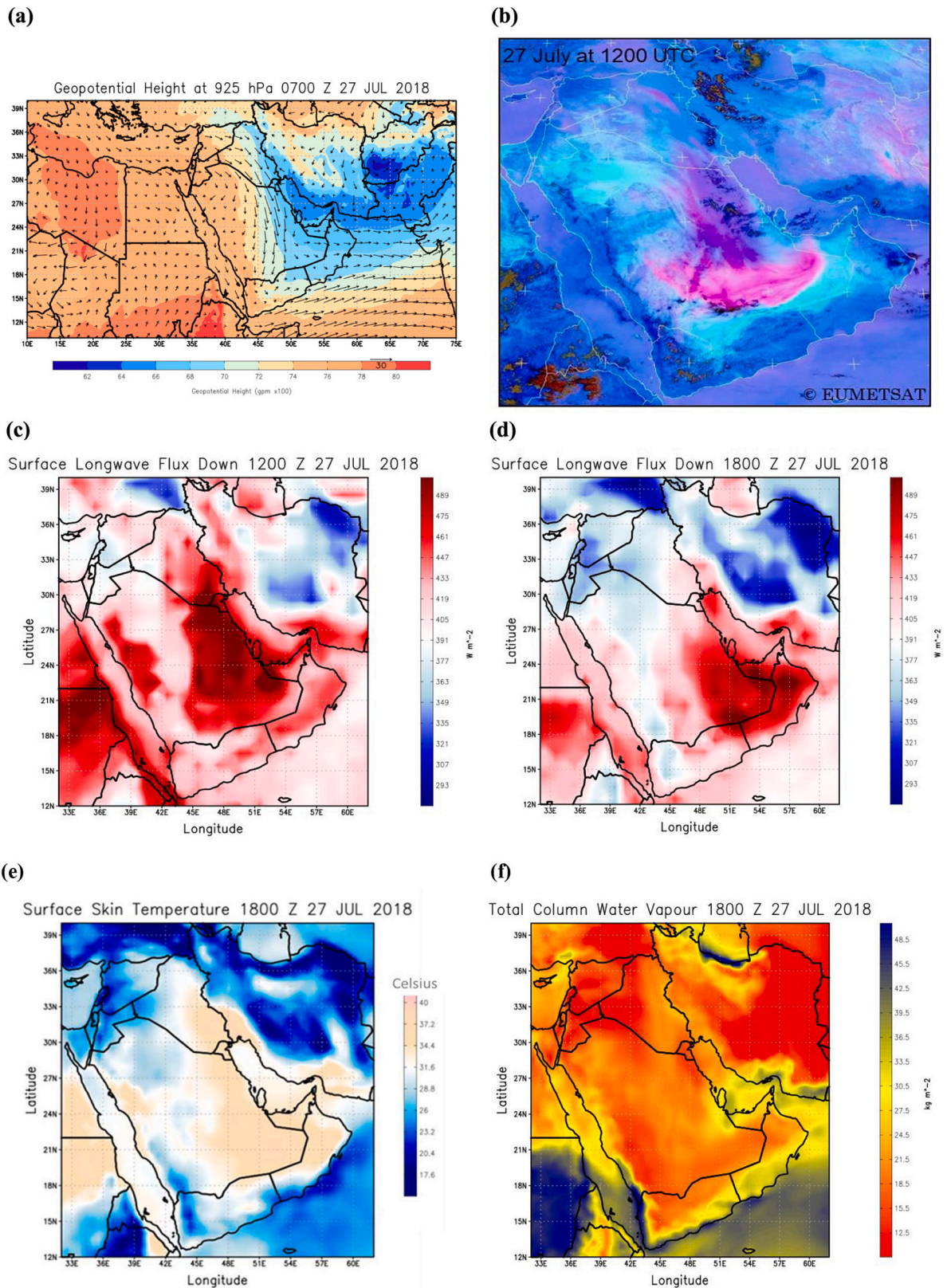


**Fig. 2.** (a) ECMWF ERA5 reanalysis on 27 July 2018 at 0700 UTC of Geopotential height at 925 hPa (colors) and wind direction (vectors) at 850 hPa. (b) SEVIRI-derived false color image on 27 July 2018 at 1200 UTC showing dust (pink/purple), clouds (brown/red) and differences in surface emissivity retrieved in the absence of dust or clouds (light blue/blue). (c) Downwelling LW fluxes at the surface derived from CERES-SYN data on 27 July 2018 at 1200 UTC. (d) Same as (c) but at 1800 UTC (10 pm local time). (e) ERA5 reanalysis of surface skin temperature on 27 July 2018 at 1800 UTC. (f) ERA5 reanalysis of total column water vapor on 27 July 2018 at 1800 UTC.

July 2018 and throughout the night on 28 July 2018. Maps of total column water vapor (TCWV) derived from ERA5 reanalysis showed continuous intrusions of maritime air masses characterized by a TCWV of  $40 \text{ kg m}^{-2}$  from the southwestern Arabian Gulf and the northwestern Arabian Sea towards the AP where the dry atmospheric column was associated with a TCWV content below  $20 \text{ kg m}^{-2}$  (Fig. 2f). The advance inland of moist air masses was also visible in the SEVIRI imagery (Fig. 2b) where moist atmosphere was observed along the AP coast and was associated with darker blue colors.

The dust storm continued its southward propagation by the Shamal winds throughout the night on 27 July 2018 (Fig. 3a). The thick dust cloud induced a net instantaneous radiative warming of  $+25 \text{ W m}^{-2}$  at the surface over land during night (Fig. 3b). This warming increased the skin temperature and favored a steeper surface-temperature gradient ( $14^\circ \text{C}$ ) along the interface between the dusty atmosphere inland and the moist atmosphere over surrounding seas (Fig. 3c), which enhanced the propagation of moist air masses inland and generated a stronger convergence between these flows. Maritime air masses emanating from the southwestern Arabian Gulf and northwestern Arabian Sea and characterized by 2-m specific humidity values up to  $16 \text{ g/kg}$  (Fig. 3d, e) propagated inland towards the desert and converged along the hot band of dust now located over southwestern United Arab Emirates (UAE) and parts of southeastern Saudi Arabia over the Empty Quarter Desert. These moist intrusions, converging over the desert, were characterized by TCWV of  $45 \text{ kg m}^{-2}$  whereas the TCWV of the surrounding atmosphere did not exceed  $20 \text{ kg m}^{-2}$  (Fig. 3f).

### 3.2. Cyclone development and associated dust storm during 28–31 July 2018

On 28 July 2018 thick dust cloud blanketed most of Yemen, Oman and southern Saudi Arabia (Fig. 4b). Because of the confluence between the northeasterly winds and the Somali jet over the Arabian Sea (Fig. 2a), the dust was accumulated along the region of convergence between these two flows (i.e., Rashki et al., 2019). The concentrated dust along the convergence zone induced a radiative warming at the surface along its footprint via the increase in LW at the surface especially during night (Fig. 2d) which derived moist air from the surrounding seas towards the desert.

The increased frontogenesis between the hot and dry atmosphere over desert and the flow of moist intrusions from the Arabian Gulf and the Arabian Sea favored the formation of a cyclone over southwestern UAE centered at  $54^\circ \text{E}$  and  $22^\circ \text{N}$  and associated with a low pressure of  $994 \text{ hPa}$  (Fig. 4a). To the east of the dust cloud generated on the previous day by Shamal winds, new dust emissions induced by strong cyclonic winds ( $12 \text{ m s}^{-1}$ ) started to occur over the UAE and northwestern Oman associated with the development of the cyclone (Fig. 4b).

The cyclone and the associated dust emissions were detected from space by the CALIOP. On 28 July 2018 at 0924 UTC, CALIPSO observations showed a layer of high reflectivity extending between  $18^\circ \text{N}$  and  $26^\circ \text{N}$  in latitudes associated with aerosols optical depth (AOD) of 3 to 5. The altitudes of the dust increased gradually from 1 km around  $26^\circ \text{N}$  to 4 km in altitudes around  $22^\circ \text{N}$  (Fig. 4c). ERA5-derived winds along the CALIPSO path revealed strong updraft and horizontal convergence around the cyclone center at  $22^\circ \text{N}$ . A potential temperature gradient of  $18 \text{ K}$  can be seen at the front between the cold and the warm fronts of the cyclone. The strong winds associated with the cold front occurred in a layer between the surface and up to 3 km in altitudes, whereas the northeasterlies expanded up to 5 km (Fig. 4c). The vertical transport of dust up to 4 km was favored by strong updraft near the cyclone center and occurred between  $21^\circ \text{N}$  and  $24^\circ \text{N}$  (Fig. 4c). This is consistent with previous studies characterizing dust emissions associated with cyclones over North Africa (e.g., Bou Karam et al., 2010; Francis et al., 2018, 2019a) and over the Middle East (Francis et al., 2019c).

The dust emissions associated with the cyclone intensified on 29 July 2018 (Fig. 5a), and the center of the cyclone moved southward by 1

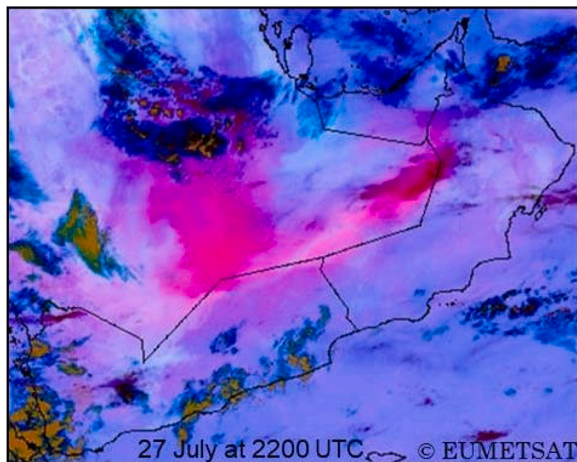
degree with a low-pressure center ( $994 \text{ hPa}$ ) located at  $54^\circ \text{E}$  and  $21^\circ \text{N}$  over the Empty Quarter Desert (Fig. 5b). Thick dust clouds in cyclonic shape are seen in MODIS (Fig. 1) and SEVIRI images (Fig. 5a) covering most of Oman, the UAE and parts of the Arabian Sea. The intensification of the cyclone dynamically forced additional moist intrusions from the Arabian Gulf and the Arabian Sea. Plumes of moisture continued to advance into the dry and hot atmosphere over the desert (Fig. 5c). The availability of moisture over land combined with the strong convergence of confluent flows and strong updraft associated with the dynamic of the cyclone, favored the development of clouds on top of the dust layer (Fig. 5d). The freshly emitted dust aerosols may have also served as cloud condensation nuclei (e.g., Karydis et al., 2011). In addition, the dust radiative impact may have deepened the low-pressure further (e.g., Chen et al., 1994), leading to enhanced moisture intrusions during night, stronger surface winds and subsequently, larger dust emissions. Previous studies on dust impact on the parent cyclone (e.g., Chen et al., 1994) have shown that the feedback of dust heating not only warms the atmosphere in the dust region but also enhances the adiabatic baroclinic forcing, leading to stronger low-level frontogenesis and stronger cyclone (e.g., Kaskaoutis et al., 2019a). The low-level front associated with the dust storm can be strongly intensified by the dust radiative heating and the dust related thermal forcing can significantly affect the evolution of the cyclone and the dust storm (e.g., Chen et al., 1994).

The dust storms generated by the cyclone resulted in satellite-derived aerosol optical depth (AOD) at  $10 \mu\text{m}$  of 1 on 29 July 2018 at 2100 UTC (Fig. 6a), a mean dust-cloud height of 5 km along the warm front of the cyclone and a 2 km mean-height along its cold front (Fig. 6c). On 30 July 2018, the dusty cyclone expanded horizontally and moved towards southern Oman (Fig. 5d). AERIOIASI satellite product showed on that day a more symmetric structure in altitude with 5 km mean dust-height in all the areas of the cyclone (Fig. 6d) and AOD above 1 (Fig. 6b). The 3D-distribution of dust aerosols derived from AERIOIASI satellite observations shows a thick and continuous band of dust expanding from the surface to 5 km in altitude around the center of the cyclone which was located above the UAE and the Empty Quarter Desert (Fig. 6e, f). A spiral band of dust associated with the cyclone outflow at higher altitudes is seen at the regions away from the cyclone center (i.e., over Oman and the Arabian Sea). This band of dust was detached from the surface and reached 6 km in altitudes (Fig. 6e, f), which may have facilitated the long-range southward transport of the uplifted dust.

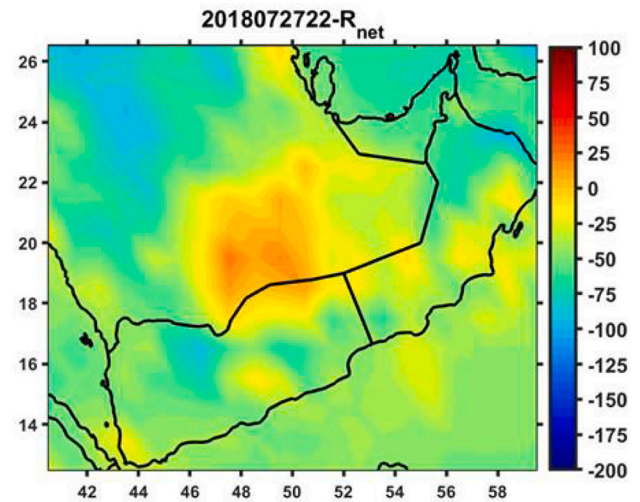
### 3.3. Cloud and rain development over the desert

On the second day of the cyclonic episode, clouds started to develop in the warm sector of the cyclone. In the afternoon on 29 July 2018, shallow clouds formed on top of the dust layer (Fig. 5d). Localized rain occurred on that day as was reported at the weather stations located in southwestern UAE. The intensification of the cyclone on 30 July 2018 derived additional moist intrusions from the Arabian Gulf and the Arabian Sea (Fig. 7a, b) which favored the development of convection and additional rain throughout the day on 30 July 2018 (Fig. 7c, d). A few convective clouds are seen over southern UAE and the Empty Quarter Desert and a line of convective cells along the Al Hajar Mountains in the UAE and Oman (Fig. 7c, d) where orographic forcing facilitated at the development of several cells. A CALIPSO path occurred over the cyclone on 30 July 2018 at 0900UTC and allowed a characterization of the vertical structure of the boundary layer during these unstable conditions. The thick dust layer seen in SEVIRI (Fig. 7c) was associated with AOD higher than 3 and stretched between 3 km and 5 km in altitude over land (i.e., between  $21^\circ \text{N}$  and  $23^\circ \text{N}$ ) and between 2 km and 4 km in altitude over the Arabian Sea (i.e., between  $16^\circ$  and  $21^\circ \text{N}$ ), hence covering in total 7 degrees in latitudes (Fig. 7e). North to  $23^\circ \text{N}$ , a highly-reflective low-level layer of aerosols expanding between the surface and 3 km in altitude, covered the Sea of Oman and the Iranian coast and may have been associated with a mixture of dust, sea salt and polluted aerosols. Strong low-level winds between the surface and 2 km in

(a)

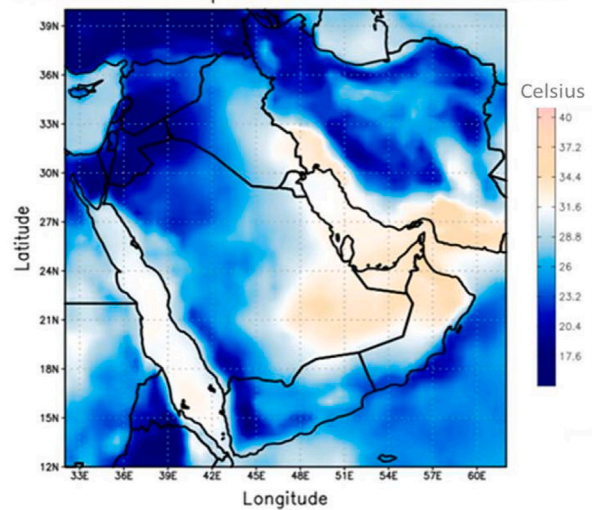


(b)



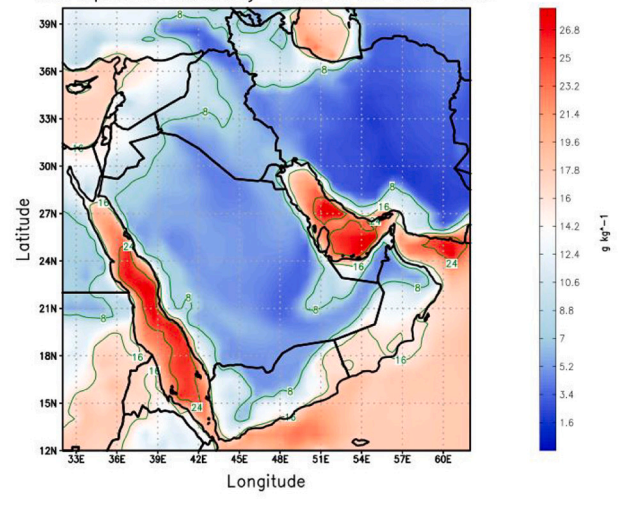
(c)

Surface Skin Temperature 0300 Z 28 JUL 2018



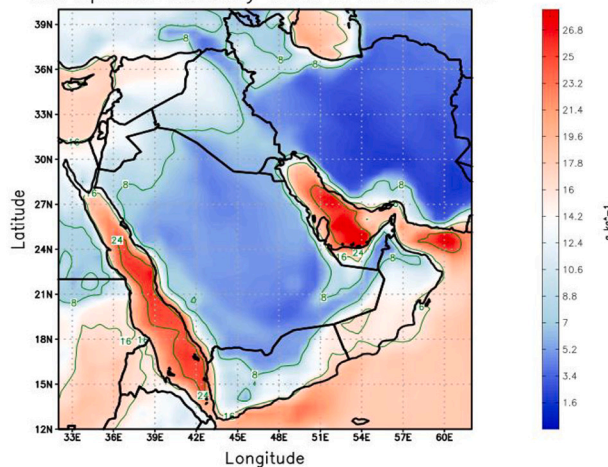
(d)

2m Specific Humidity 0000 Z 28 JUL 2018



(e)

2m Specific Humidity 0400 Z 28 JUL 2018



(f)

Total Column Water Vapour 1000 Z 28 JUL 2018

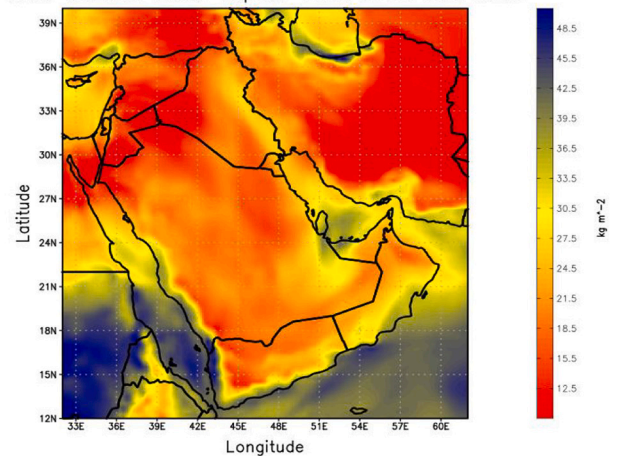


**Fig. 3.** (a) SEVIRI-derived false color image on 27 July 2018 at 2200 UTC showing dust (pink/purple), clouds (brown/red) and differences in surface emissivity retrieved in absence of dust or clouds (light blue/blue). (b) Surface net radiation derived from CERES-SYN satellite data on 27 July 2018 at 2200 UTC. (c) ERA5 reanalysis of surface skin temperature on 28 July 2018 at 0300 UTC. (d) RA5 reanalysis of 2-m specific humidity on 28 July 2018 at 0000 UTC. (e) Same as (d) but on 28 July 2018 at 0400 UTC. (f) ECMWF ERA5 reanalysis of total column water vapor on 28 July 2018 at 1000 UTC.



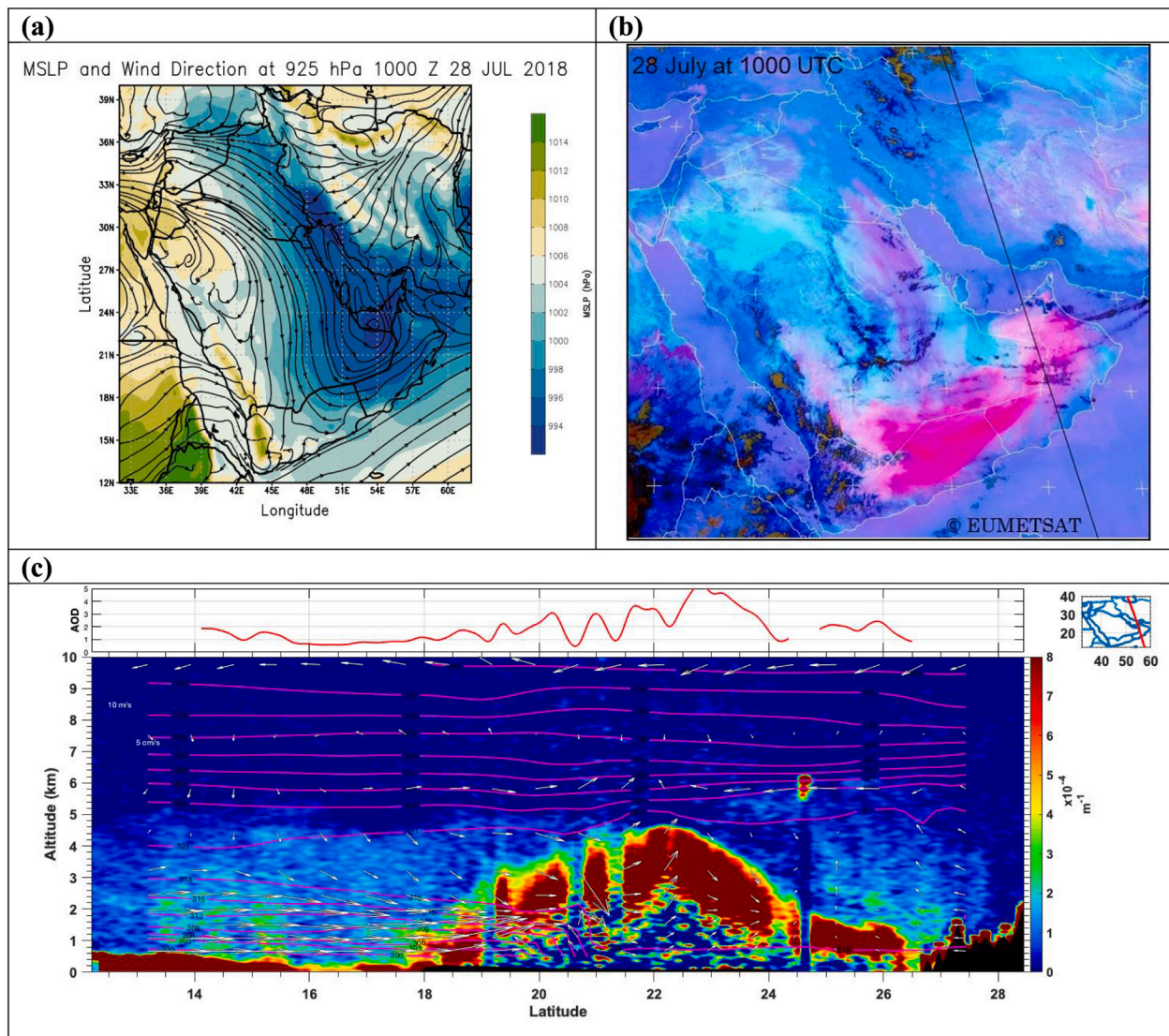


**Fig. 4.** (a) ECMWF ERA5 reanalysis of mean sea level pressure (shaded) and wind direction at 925 hPa superimposed in streamlines on 28 July 2018 at 1000 UTC. (b) SEVIRI-derived false color image on 28 July 2018 at 1000 UTC showing dust (pink/purple), clouds (brown/red) and differences in surface emissivity retrieved in absence of dust or clouds (light blue/blue). (c) CALIPSO observations along the black line on (b) of aerosol extinction coefficient at 532 nm on which are superimposed the wind direction in vectors and the isentropes derived from ECMWF ERA5 reanalyses along the CALIPSO track. CALIPSO-derived AOD at 532 nm are shown in the upper panel on (c).

altitude were seen along the CALIPSO track between 16°N and 24°N to be associated with the cyclone front and the southerly flow (Fig. 7e). Vertical convergence between two opposing flows occurred around 25°N along the eastern flank of the Al Hajar Mountains (Fig. 7e). The development of convective cells associated with the cyclone continued during the evening of 30 July 2018 and throughout the day on 31 July 2018. Denser convective cells and their associated rain were seen to develop over the Empty Quarter Desert on 31 July 2018 (Fig. 7f, g) where the whole UAE, Oman and parts of southeast Saudi Arabia was under the influence of maritime air masses (Fig. 7a, b). ERA5 reanalysis of total precipitation indicated the occurrence of an accumulated 7 mm rain on 30 July 2018 over the Empty Quarter Desert (not shown).

#### 4. Radiative impact of the dust storm associated with the cyclone

The radiative impact of the dust storm generated by the cyclone is assessed in this section based on ground-based and satellite observations. The Al Ain station is located at the northern periphery of the thick

dust cloud (Fig. 1). Despite being outside the dense layer of dust, observations at this location showed a clear impact of the dust storm on the radiative fluxes and temperature (Fig. 8).

The diurnal cycle of the temperature at the surface was strongly altered by the dust radiative forcing. During daytime, the highest temperatures observed during the dust storm period were 2 °C higher compared to the maximum of temperature registered on the days preceding the dust storm (Fig. 8a). At night, the lowest temperatures observed during the dust storm were 10 °C higher compared to night minima in temperature before and after the dust storm (Fig. 8a). This significant increase in surface temperatures was due to sustained emissions of longwave radiation by the dust clouds during the entire lifetime of the dust storm. Despite a strong reduction during daytime in the SW fluxes at the surface (between  $-300 \text{ W m}^{-2}$  on 28 July 2018 and  $-400 \text{ W m}^{-2}$  on 30 July 2018 i.e., Fig. 8b), the strong increase in LW radiation fluxes resulted in a warming effect at the surface. The downwelling LW fluxes during the 4-day dust storm period increased significantly both during day ( $+60 \text{ W m}^{-2}$ ) and during night ( $+100 \text{ W m}^{-2}$ ), compared to the values registered outside this period (Fig. 8c). Consequently, the

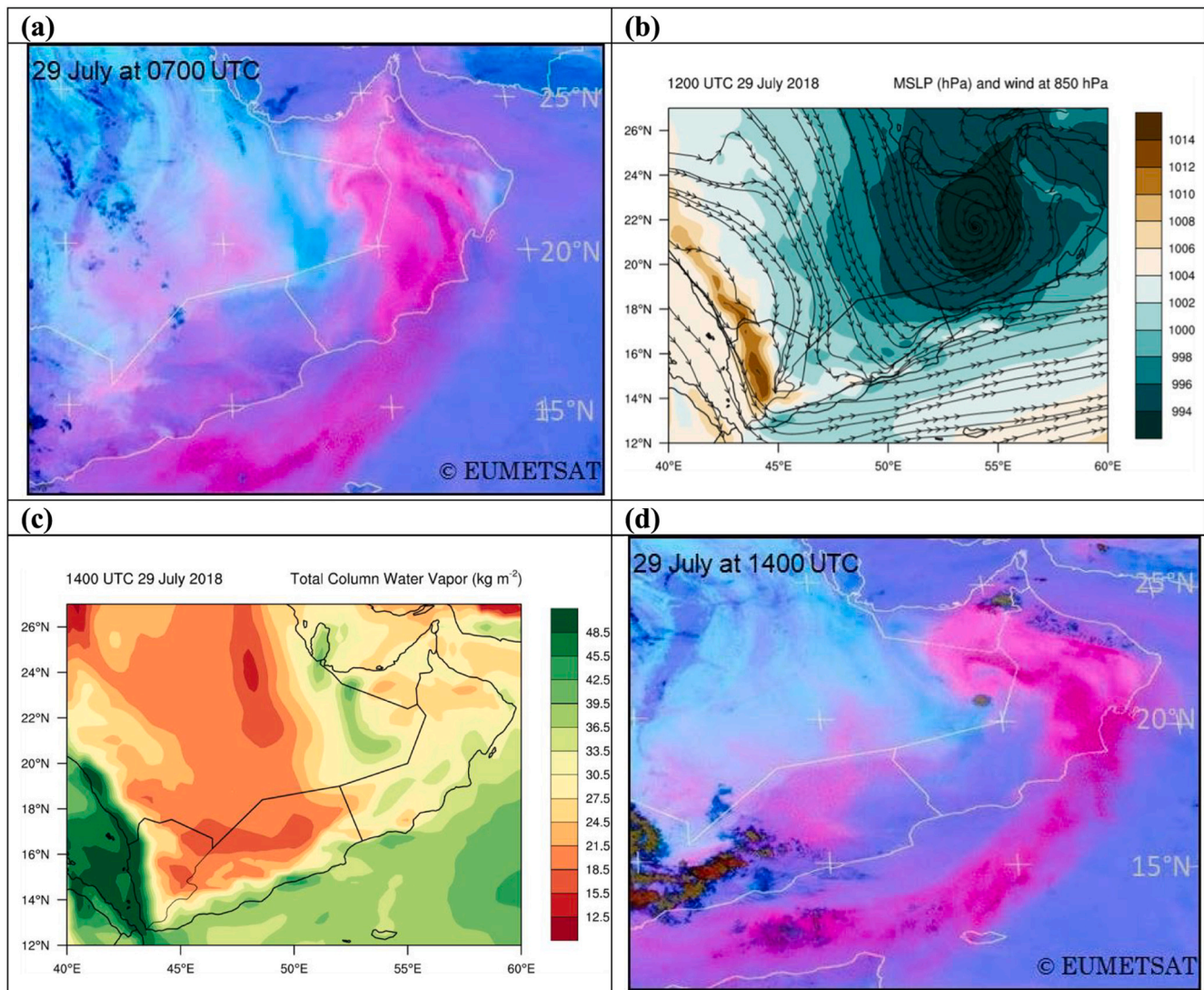


Fig. 5. (a) SEVIRI-derived false color image on 29 July 2018 at 0700 UTC. (b) ECMWF ERA5 reanalyses of mean sea Level pressure (colors) and wind direction at 925 hPa (streamlines) on 29 July 2018 at 1200 UTC. (c) ERA5 reanalyses of total column water vapor on 29 July 2018 at 1400 UTC. (d) Same as (a) but at 1400 UTC.

diurnal cycle of the net radiation fluxes at the surface was marked by a decrease of  $-100 \text{ W m}^{-2}$  in the daily maximum and an increase of  $+50 \text{ W m}^{-2}$  in the nighttime minimum (Fig. 8d). Although these competing effects mean that the net surface radiative flux reduction is small, the diurnal effects are pronounced, with the dust SW apparent in daytime and the LW effect dominant at night, which has implications on the evolution of the planetary boundary layer (e.g., Maghrabi and Al-Dosari, 2016) and on mesoscale atmospheric circulations such as sea breeze (e.g., Alamirew et al., 2018).

At Gasyoura station, a location closer to the core of the dust storm (Fig. 1), the signatures of the dust radiative forcing observed at Al Ain were more pronounced (Fig. 9). Temperatures during night did not go below  $37^\circ\text{C}$  being  $11^\circ\text{C}$  higher than nocturnal-temperature lows before and after the dust storm (Fig. 9a). However, the maximum in temperature during day decreased by  $3^\circ\text{C}$  (Fig. 9a) due to the reduction in SW radiation at the surface by the thick layer of dust. Indeed, the dust cloud induced a maximal SW reduction of  $-400 \text{ W m}^{-2}$  at the surface on 29 and 30 July 2018 (Fig. 9b), similar to the findings by previous studies on spring dust storms over central AP (Prakash et al., 2015) and over the UAE (Karagulian et al., 2019). At this station, there was no measurements of the LW radiation fluxes. However, from the temperature variation and based on the measurements at Al Ain, we think that the

dust clouds induced a comparable or slightly higher increase in LW radiation at Gasyoura compared to Al Ain. The alteration of the radiative budget by the dust impacted the atmospheric boundary layer and the circulation. The observations of surface winds at Gasyoura registered calm conditions during day with a  $5 \text{ m. s}^{-1}$  decrease in the daily maximum of wind speed during the period of the storm (Fig. 9c). There was a shift in high wind conditions towards night and early morning hours during the dust storm. This change in the behavior of winds may reflect previous findings pointing to the fact that dust tends to stabilize the boundary layer during the day but induce instability during night (e.g., Zhao et al., 2011). The pressure at the surface on the day of the formation of the cyclone (i.e., 28 July 2018) over southwestern UAE dipped to 996 hPa at Gasyoura (Fig. 9d) and the relative humidity was very low around 20%, but increased gradually during the rest of the period to reach 60% on 31 July 2018 (Fig. 9d). When the cyclone moved southward on the day following its formation, it entrained with it the intrusion of moist air from the Arabian Gulf further inland. The dynamically forced maritime air masses by the cyclone were able to reach interior regions in the UAE such as Gasyoura and contribute therefore to cloud and rain development.

The observed radiative impact at certain locations was also present over the whole area affected by the dust storm and even more

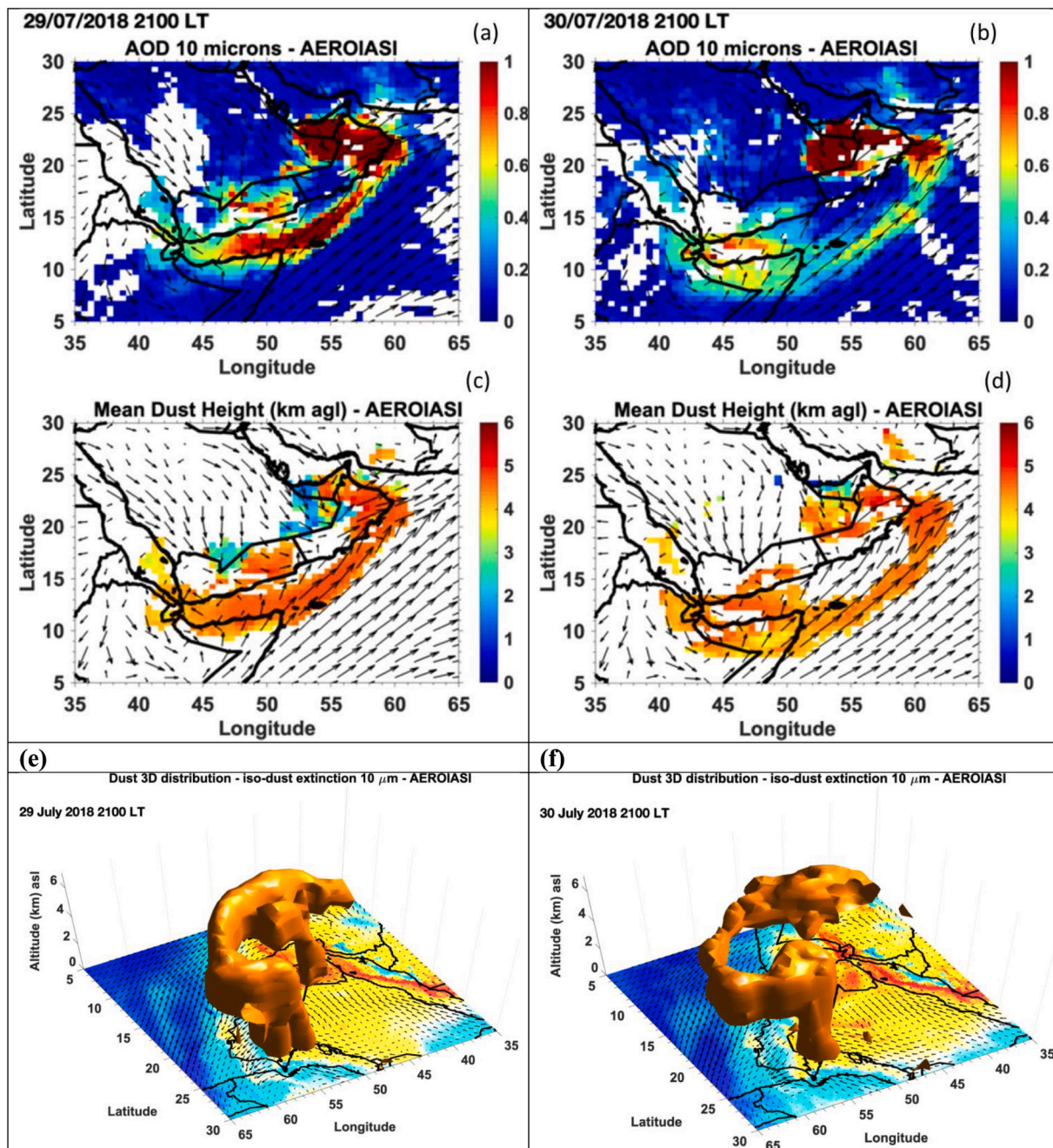


**Fig. 6.** AEROIASI derived maps of: (a) Aerosol optical depth (AOD) at 10  $\mu\text{m}$  on 29 July 2018 at 2100 LT. (b) Same as (a) but on 30 July 2018 at 2100 LT. (c) Mean height of dust layers in km on 29 July 2018 at 2100LT. (d) Same as (c) but on 30 July 2018 at 2100 LT. (e) Satellite-derived 3D distribution of dust aerosols on 29 July 2018 at 2100UTC. (f) Same as (e) but on 30 July 2018 at 2100 UTC. ERA5 10-m winds are superimposed in black vectors.

pronounced over the regions close to the core of the dust storm with thick dust plumes. Satellite observations of radiative fluxes collocated with Al Ain and Gasyoura stations show a good agreement between the CERES-SYN fluxes and those measured at the ground (Figs. 8 and 9). The 2D maps of radiative fluxes derived from CERES-SYN show a clear footprint of the dust storm at the surface with a decrease in the net surface radiation during day due to the absorption and reflection of shortwave radiation by the dust layer and an increase in net surface radiation during night due to the increased in LW re-emission (Fig. 10). The footprint of the dust cyclone was visible in the radiative observations; the daytime reduction and the nighttime increase in the net radiation at the surface followed the southward propagation of the cyclone (Figs. 7, 10). The instantaneous net radiation at the surface was reduced by  $-200 \text{ Wm}^{-2}$  during the day, compared to values at the surrounding

areas outside the footprint of the dust storm (Fig. 10a, c, d). This was largely due to the reduced shortwave flux from atmospheric absorption. At the same time, the instantaneous net radiation at the surface was increased at by  $+175 \text{ Wm}^{-2}$  (Fig. 10b, d, e) largely due to increase in re-emission of longwave radiation (Fig. 10h). This opposite effect of dust on the surface radiation between day and night tends to stabilize the atmosphere during daytime and reduce the stability during the nighttime (e.g., Zhao et al., 2011). The absorption of LW radiation by the dust layer was visible in the satellite observations of LW at the TOA during day (Fig. 10g). More than  $60 \text{ Wm}^{-2}$  LW radiation was retained in the atmosphere as implied by the reduction in the LW fluxes at the TOA (Fig. 10g), leaving a cyclonic footprint at the surface underneath the cyclone and the associated dust.

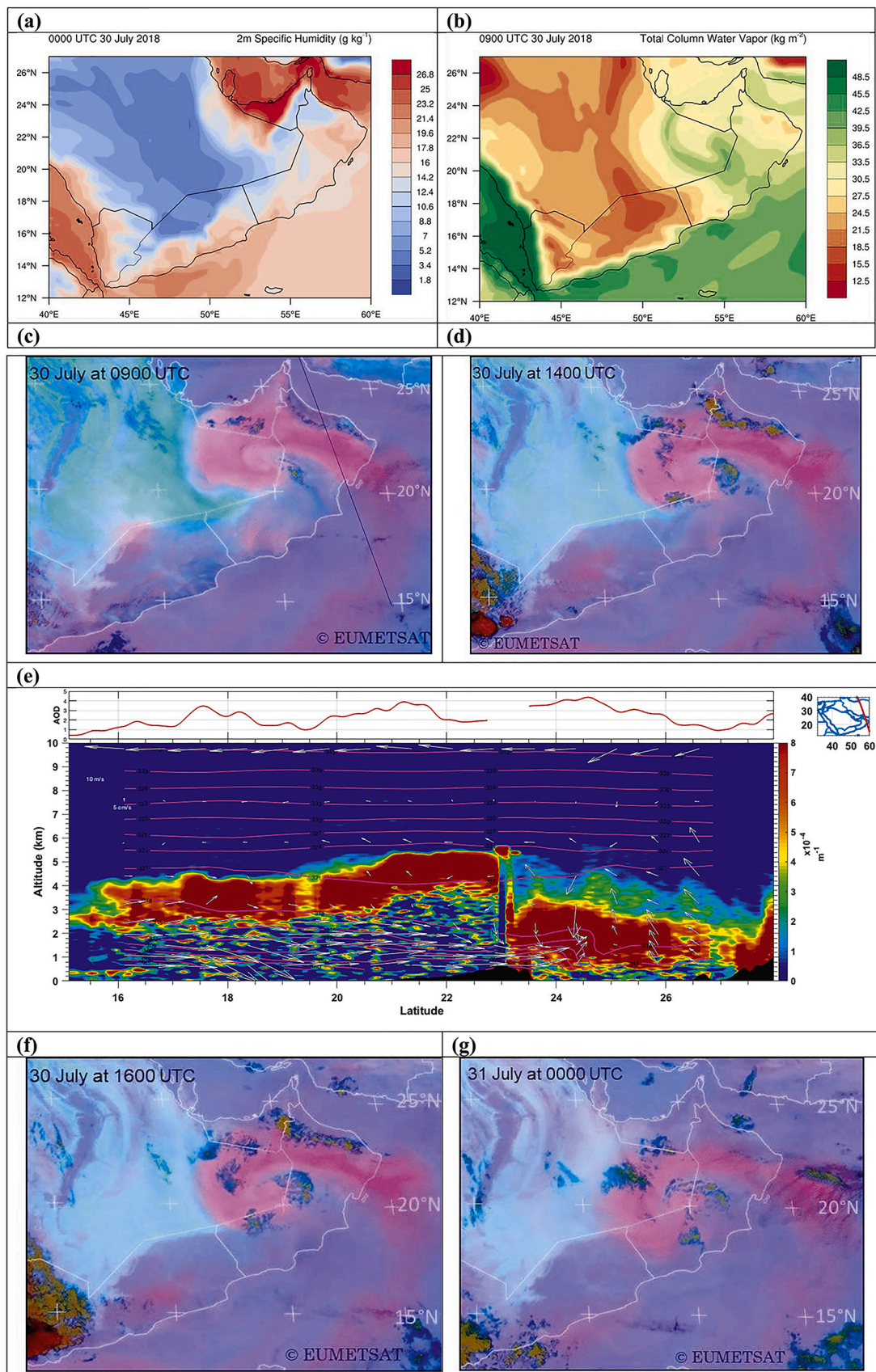


Fig. 7. - ERA5 reanalyses maps on 30 July 2018 of: (a) Specific humidity at 00UTC and (b) total column water vapor at 0900 UTC. - SEVIRI images on 30 July 2018 at 0900 UTC (c), 1400 UTC(d), 1600 UTC (f) and on 31 July 2018 at 0000 UTC (g). - On (e) CALIPSO observations on 30 July 2018 at 0900 UTC along the black line on (c) of aerosol extinction coefficient at 532 nm on which are superimposed the wind direction in vectors and the isentropes derived from ERA5 along the CALIPSO track. CALIPSO-derived AOD at 532 nm are shown in the upper panel on (e).

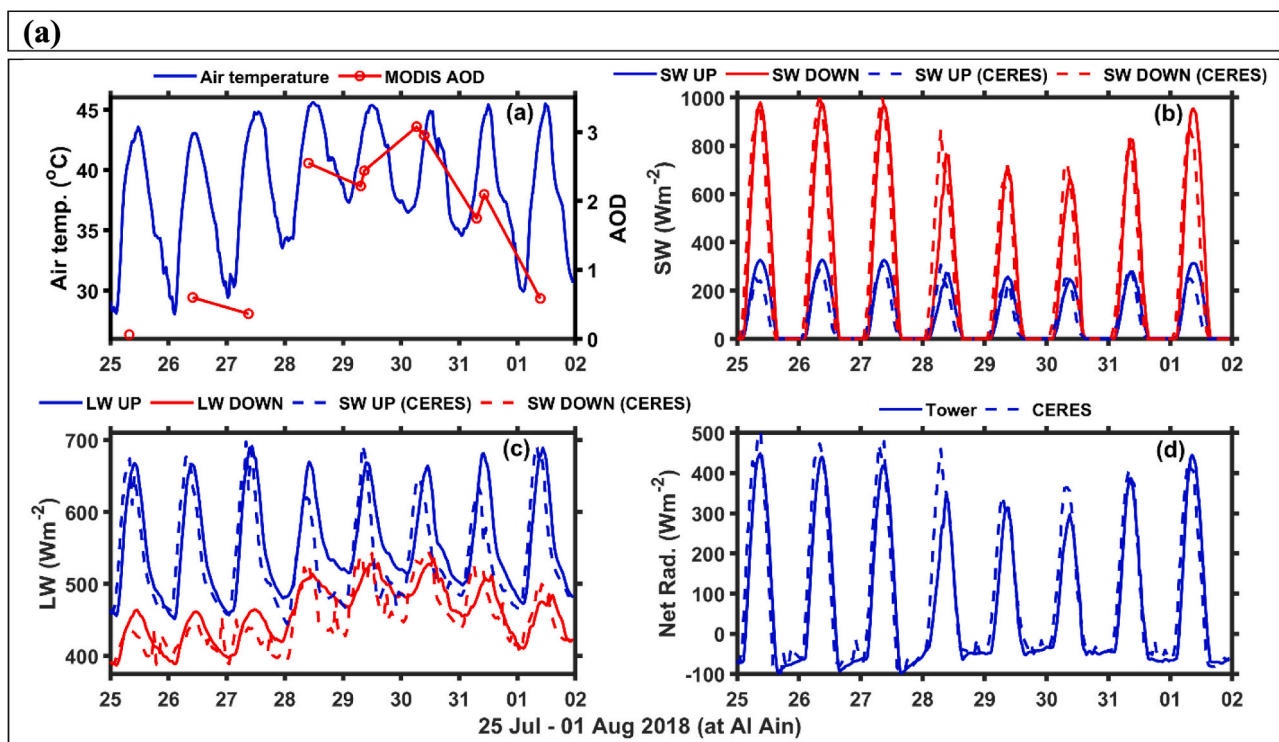


Fig. 8. Ground-based observations at Al Ain (solid lines) and collocated CERES-SYN satellite observations (dahed lines) during 26 July 2018 and 01 August 2018 of: (a) 2-m temperature and collocated MODIS Aerosol Optical Depth (AOD), (b) SW downwelling and upwelling fluxes, (c) LW downwelling and upwelling fluxes, and (d) net radiative fluxes.

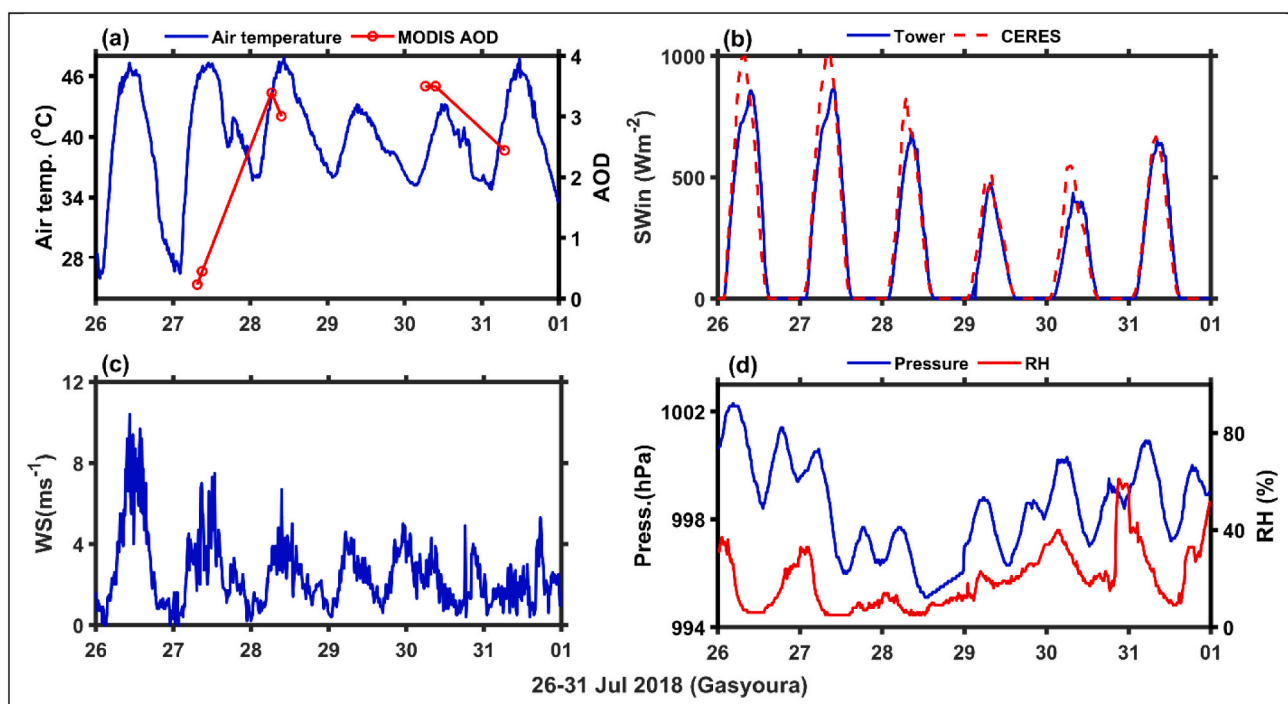


Fig. 9. Ground-based observations at Gasyoura during 26 July 2018 and 01 August 2018 of (a) 2-m temperature in blue and collocated MODIS Aerosol Optical Depth (AOD) in red, (b) SW downwelling fluxes at the surface (blue) and collocated CERES-SYN satellite observations (red), (c) wind speed, and (d) pressure and relative humidity.

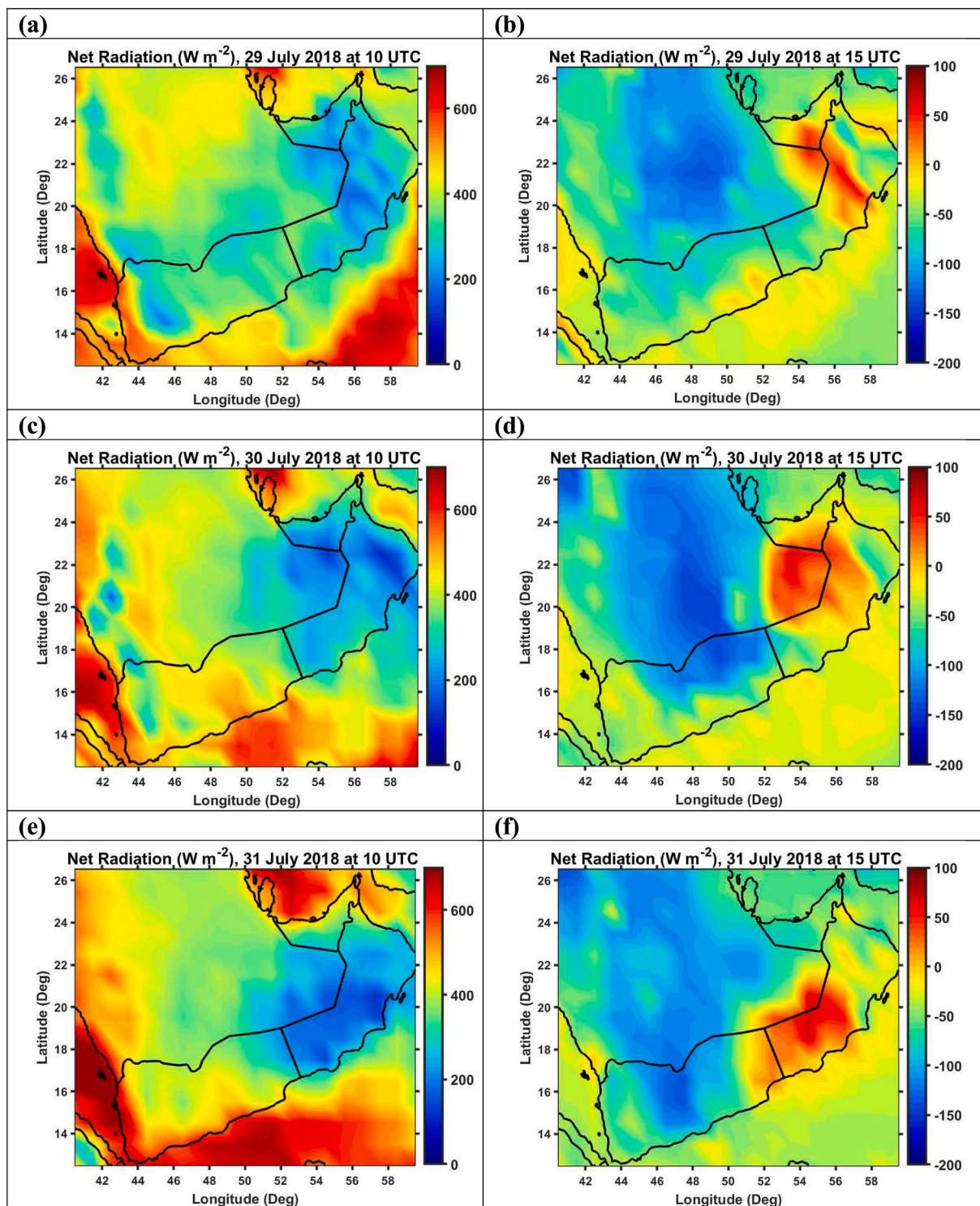


Fig. 10. Surface net radiation flux ( $W m^{-2}$ ) derived from the CERES-SYN satellite on 29 July 2018 at (a) 10 UTC (14 Local Time) and (b) 15 UTC (19 Local Time). (c)-(d) and (e)-(f) are as (a)-(b) but on 30 and 31 July, respectively. (g) CERES-SYN satellite TOA upward longwave radiation flux ( $W m^{-2}$ ) on 29 July 2018 at 15 UTC (19 LT), and (h) surface downward longwave radiation flux ( $W m^{-2}$ ) on 30 July 2018 at 03 UTC (07 LT).

## 5. Simulation of the dust storms and their radiative impact

The Meso-NH model was used to simulate the dust storm, quantify the dust load associated with it and assess the model capability in simulating the dust radiative impact (see details in Section 2). The AOD simulated by Meso-NH on 30 July 2018 was in the order of 3.6

(Fig. 11a); similar to the AOD observed by CALIPSO (Fig. 7e). The horizontal distribution of the dust storm was well captured by the model with a cyclonic shape apparent in the AOD map (Fig. 11a) and the dust load maps (Fig. 11b). However, the model positioned the center of the cyclone 2 degrees to the west of the observed SW location (Fig. 11) which could be due to the overestimation of the SW reduction. The dust load

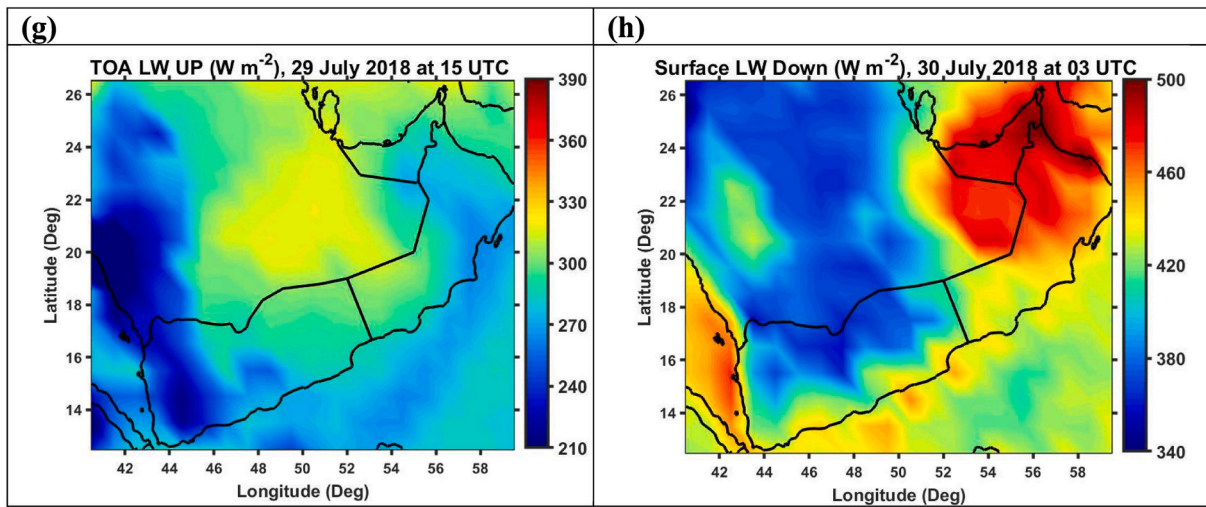


Fig. 10. (continued).

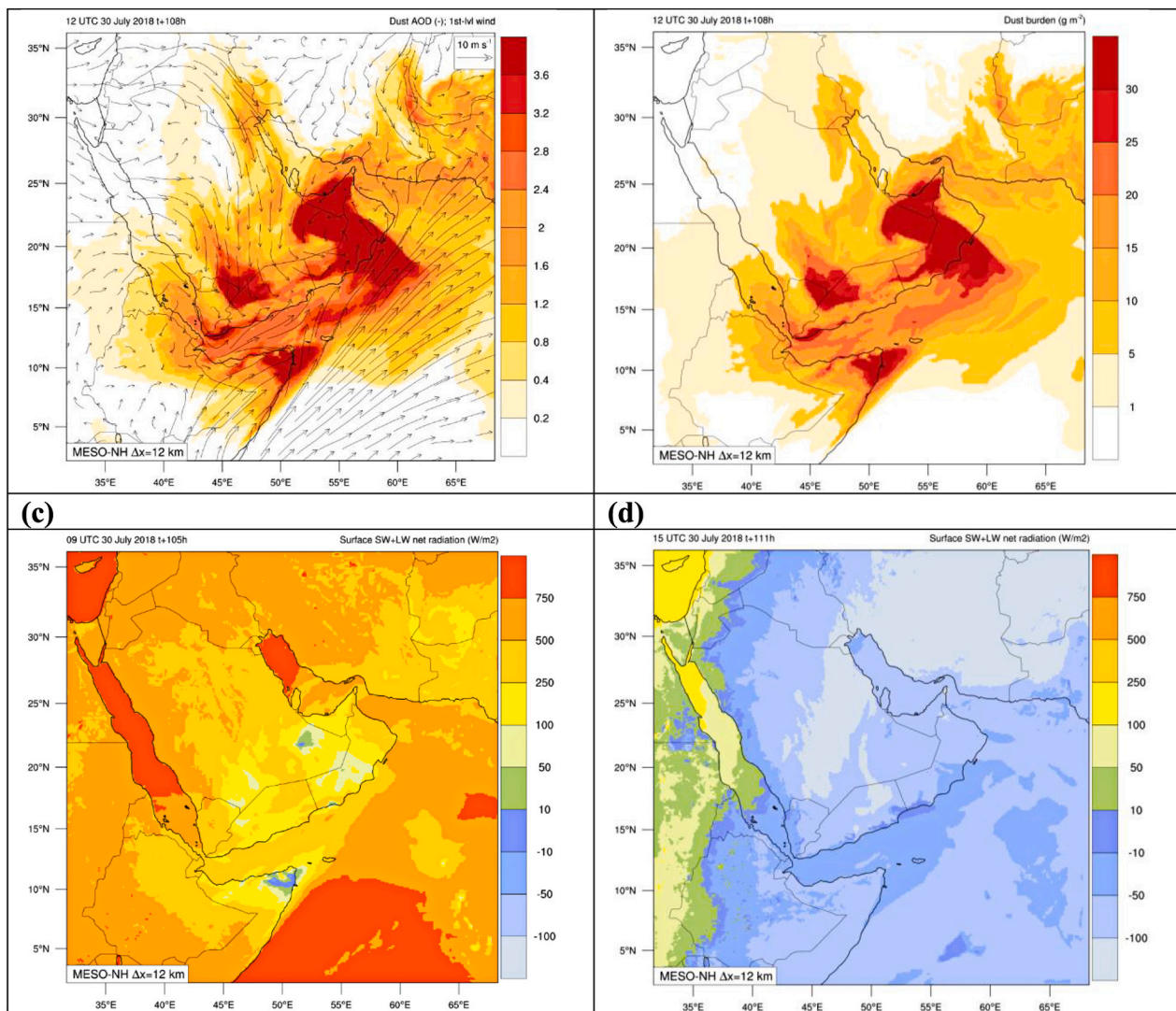


Fig. 11. Meso-NH simulations on 30 July 2018 at 1200 UTC of (a) aerosol optical depth (AOD) in colors and winds at the model first level in vectors, (b) dust loads, (c) surface net radiation on 30 July 2018 at 0900 UTC, and (d) surface net radiation on 30 July 2018 at 1500 UTC. 0900 UTC in Fig. 11c, i.e. correspond to 13 h00 local time and 1500 UTC in Fig. 11d, i.e. correspond to 19 h00 local time.

associated with the dust storm was estimated by the model to be more than  $30 \text{ g}^{-2}$  which correspond roughly to 20 Tg on average over the cyclone area.

The observed dust-induced reduction in the net radiation at the surface during daytime was well simulated by the model (Fig. 11c) with a simulated  $-400 \text{ Wm}^{-2}$  decrease in the net radiation at the surface. However, the model was not able to simulate the increase in the net radiation at the surface during night and no signature of the dust storm at the surface in the radiation field (Fig. 11d). The underestimation of the warming effect of dust by global models has been highlighted recently and was attributed to the underestimation of the amount of coarse dust particles produced and maintained in the atmosphere near source areas (Adebisi and Kok, 2020). This also seems to be the case for mesoscale models being built more or less on similar parametrizations. Indeed, the coarse dust particles produced by the Meso-NH model remain close to the surface and deposit rapidly (not shown), which could partly explain the too weak warming effect in the LW.

The comparison between the model and the observations at the two stations Al Ain (Fig. 12a) and Gasyoura (Fig. 12b) shows an overall good agreement between the model and the observations in the SW. In the LW, the model simulates well the increasing tendency during the dust storm period, but it underestimates the magnitude of the LW down at the surface by almost  $100 \text{ Wm}^{-2}$  and the LW up by  $50 \text{ Wm}^{-2}$  (Fig. 12). This underestimation of the dust-induced warming resulted in a cold bias during night in the simulated 2-m temperature of more than  $-8 \text{ }^\circ\text{C}$  at Al Ain (Fig. 12a) and  $-10 \text{ }^\circ\text{C}$  at Gasyoura (Fig. 12b). The maximum in temperature was relatively well captured by the model at Al Ain (Fig. 12a) but the cold bias persistent as well during the day at Gasyoura (Fig. 12b); the station that is closer to the core of the dust storm (Fig. 1). Here, the model also overestimated the SW reduction by  $300 \text{ Wm}^{-2}$  compared to the observations on 28 July 2018 (Fig. 12b). Similar results were obtained at 5 other stations around the two stations discussed here (not shown).

Given the fact that the model simulated reasonably well the AOD and the location of the dust storm, the discrepancy in simulating the impact of dust aerosols on radiation may come from a misrepresentation of the size distribution of the dust particles and their optical properties. These results stress the need for an observation network of these parameters near dust source regions in order to enhance our capabilities to constrain the model parametrizations and address the discrepancy in the interactions between dust aerosols and radiation.

## 6. Conclusions

In this study, we investigated the atmospheric dynamics associated with intense dust storms in summer 2018 over the AP and assessed, for the first time, their direct and semi-direct radiative effect using high-resolution in-situ and satellite observations. We identified cyclogenesis over the Empty Quarter Desert as an important mechanism for intense dust storms. This mechanism is reported here for the first time over this major source region.

We found that a surge in Shamal winds, in response to an amplified east-west pressure gradient, caused a first intense dust storm over the Arabian Peninsula. This dust storm induced significant warming at the surface during night due to the increase in longwave radiation, which warmed the surface over land and triggered the intrusion of maritime air masses from the Arabian Gulf towards the desert. Due to the confluence between two opposing winds; namely the northerly Shamal winds and the westerly Somali Jet, the dust was stagnant and accumulated along the southern coast of the AP which induced strong temperature gradient (via increase in LW) between land (warm) and sea (cold) and triggered additional surge inland of maritime air masses. The increased baroclinicity and frontogenesis over the desert along the convergence zone between the dry and hot air and the moist and relatively-cold air from the Arabian Gulf resulted in the formation of a cyclone over the Empty Quarter Desert. The cyclogenesis over this region initiated a second

intense dust storm which developed and impacted the AP for 3 consecutive days. The dust lifted by the cyclone was associated with an AOD larger than 3, reached 5 km in altitude and altered the radiative budget at the surface by inducing both significant warming during night ( $+10 \text{ }^\circ\text{C}$ ) and cooling during day ( $-3 \text{ }^\circ\text{C}$ ).

As a result of the dust-induced land/sea temperature gradient during night, additional moisture intrusions occurred over land which intensified the cyclone and generated additional i) dust emissions and ii) moist air intrusions that were dynamically entrained towards the interior desert by the cyclonic circulation. This interplay between the dust and the cyclone via direct (impact on radiation) semi-direct (impact on thermodynamics and circulation) radiative forcing set up favorable conditions for the development of convective clouds on top of the dust layer. This was promoted by the strong convergence and updrafts within the cyclone and the availability of moisture insured by the continuous moist air intrusions from the surrounding seas. The freshly emitted dust aerosols may have also served as cloud condensation nuclei and played a role in the localized rain that was reported at the ground during this 3-day summertime episode. However, only the direct and semi-direct radiative effects of dust were considered in this study, the indirect effect of dust and its interactions with clouds is to be investigated in a future work.

The dust load uplifted by the cyclone was in the order of 20 Tg as estimated by the mesoscale model Meso-NH, and associated aerosol optical depth higher than 3. The model simulates reasonably the radiative impact of the dust in the shortwave but highly underestimated its impact

in the LW. Our study stresses the importance of the dust radiative forcing in the longwave and that models must include an accurate treatment of this effect to properly represent the impact of dust on the Earth system especially near source areas.

Based on observations, we found that the dust over a major dust source region induces a significant net warming effect at the surface and in the atmosphere during night, modifying thereby the atmospheric circulation at low levels such as sea breeze (e.g., Saleeby et al., 2019). This contradicts the main findings by previous work based mainly on numerical models, where it was found that the dust effect is a cooling of the near-surface layers (Tulet et al., 2008; Lemaitre et al., 2010; Lavaysse et al., 2011). Our results are consistent with the recent findings by Adebisi and Kok (2020) where a net warming effect of the dust was reported and reflect the need for a better representation in the models of the effect of dust in the LW as well as an improved representation of the particle size and their optical properties.

Our results highlight the important role of dust aerosols and the extent of their impact on the different components of the climate system of the AP. Therefore, air quality and weather forecast systems need to account for the dust storm radiative impacts in order to improve their accuracy. Additionally, dust aerosols need to be considered when predicting, designing and conducting cloud-seeding operations in the UAE because of their impact on the circulation which in turn impacts the development of convective clouds and their lifetime.

Dust aerosols is a quasi-permanent natural aerosol in the atmosphere over the AR and its impact on the different components of the climate and the environment of this region is found to be more significant than previously thought. A longer term analysis of the dust activity over the AP, its drivers and the radiative impact of dust aerosols is still lacking and could be the essence of a future work.

## Author contributions

D.F. conceived the study and wrote the initial and the revised manuscript. J.P.C. performed the numerical simulations. N.N. analyzed the satellite and ground-based data. J.C. analyzed CALIPSO and AERO-IASI satellite data. N.A. analyzed the ERA5 data. M.T., O.P. and L.X. provided input on result analysis. All authors interpreted the results and provided input to the final manuscript.



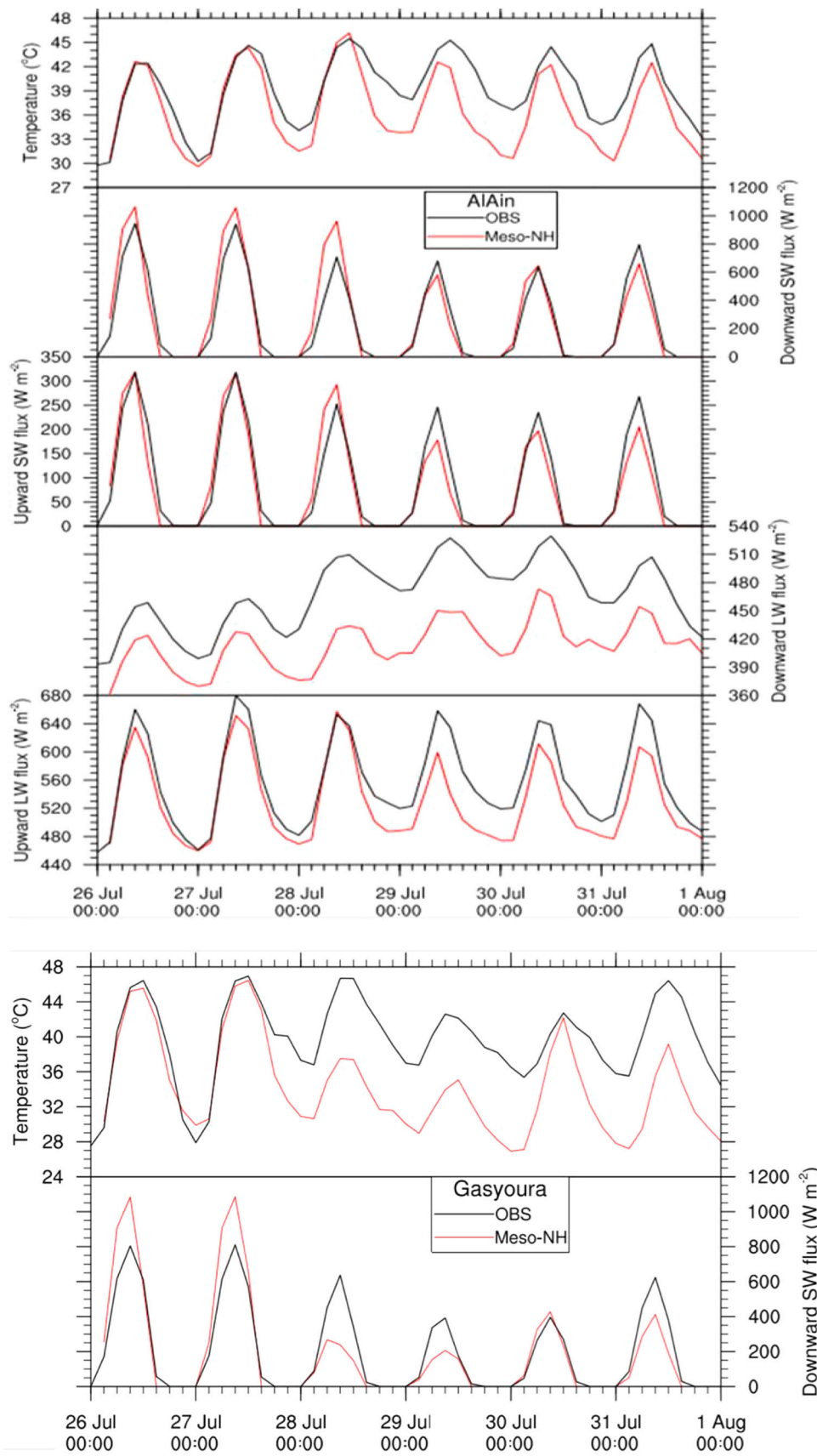


Fig. 12. Comparison between Meso-NH simulations and ground-based observations of 2-m air temperature, SW and LW fluxes during 26 July 2018 and 1 August 2018 at (a) Al Ain and (b) Gasyoura.

## Data and materials availability

All data needed to evaluate the conclusions in the paper are present in the paper. Correspondence and requests for materials should be addressed to DF.

## Declaration of Competing Interest

The authors declare that they have no competing interests.

## Acknowledgement

Part of this work is supported by the National Center of Meteorology, Abu Dhabi, UAE under the UAE Research Program for Rain Enhancement Science. We are grateful to Prof. Volker Wulfmeyer, Dr. Hans-Dieter Wizemann, and Dr. Oliver Branch from the University of Hohenheim for operating the eddy-covariance station and processing the raw measurements of radiative fluxes at Al Ain. We also want to thank the National Centre for Meteorology (NCM) in the UAE for providing observational data at Gasyoura.

## References

- Adebiyi, A.A., Kok, J.F., 2020. Climate models miss most of the coarse dust in the atmosphere. *Sci. Adv.* 6 (15) <https://doi.org/10.1126/sciadv.aaz9507>, 08 Apr 2020. eaz9507.
- Alamirew, N.K., Todd, M.C., Ryder, C.L., Marsham, J.H., Wang, Y., 2018. The early summertime Saharan heat low: sensitivity of the radiation budget and atmospheric heating to water vapour and dust aerosol. *Atmos. Chem. Phys.* 18, 1241–1262. <https://doi.org/10.5194/acp-18-1241-2018> (2018).
- Ali, A.H., 1994. Wind regime of the Arabian Gulf. In: El-Baz, F., Makhariha, R.M. (Eds.), *The Gulf War and the Environment. Gordon and Breach, New York*, pp. 31–48.
- Banks, J.R., Brindley, H.E., Hobby, M., Marsham, J.H., 2014. The daytime cycle in dust aerosol direct radiative effects observed in the Central Sahara during the Fenice campaign in June 2011. *J. Geophys. Res.-Atmos.* 119, 13861–13876. <https://doi.org/10.1002/2014JD022077>.
- Banks, J.R., Schepanski, K., Heinold, B., Hunerbein, A., Brindley, H.E., 2018. The influence of dust optical properties on the colour of simulated MSG-SEVIRI Desert Dust imagery. *Atmos. Chem. Phys. Discuss.* <https://doi.org/10.5194/acp-2018-48>.
- Bechtold, P., Bazile, E., Guichard, F., Mascart, P., Richard, E., 2001. A mass flux convection scheme for regional and global models. *Q. J. R. Meteorol. Soc.* 127, 869–886.
- Boose, Y., Welti, A., Atkinson, J., Ramelli, F., Danielczok, A., Bingemer, H.G., Plötze, M., Sierau, B., Kanji, Z.A., Lohmann, U., 2016. Heterogeneous ice nucleation on dust particles sourced from nine deserts worldwide – part 1: Immersion freezing. *Atmos. Chem. Phys.* 16, 15075–15095. <https://doi.org/10.5194/acp-16-15075-2016>.
- Bou Karam Francis, D., Flamant, C., Chaboureaud, J.-P., Banks, J., Cuesta, J., Brindley, H., Oolman, L., 2017. Dust emission and transport over Iraq associated with the summer Shamal winds. *Aeolian Res.* 24, 15–31.
- Bou Karam, D., Flamant, C., Knippertz, P., Reitebuch, O., Pelon, J., Chong, M., Dabas, A., 2008. Dust emissions over the Sahel associated with the West African Monsoon inter-tropical discontinuity region: a representative case study. *Q. J. R. Meteorol. Soc.* 134, 621–634.
- Bou Karam, D., Flamant, C., Knippertz, P., Reitebuch, O., Pelon, J., Chong, M., Dabas, A., 2009a. Dry cyclogenesis and dust mobilization in the Inter Tropical Discontinuity of the West African Monsoon: a case study. *J. Geophys. Res.* 114, D05115 <https://doi.org/10.1029/2008JD010952>.
- Bou Karam, D., Flamant, C., Knippertz, P., Reitebuch, O., Pelon, J., Chong, M., Dabas, A., 2009b. Dry cyclogenesis and dust mobilization in the Inter Tropical Discontinuity of the West African Monsoon: a case study. *J. Geophys. Res.* 114 (D05115).
- Bou Karam, D., Flamant, C., Cuesta, J., Pelon, J., Williams, E., 2010. Dust emission and transport associated with a Saharan depression: the February 2007 case. *J. Geophys. Res.* <https://doi.org/10.1029/2009JD012390>.
- Bou, Karam D., Williams, E., Janiga, M., Flamant, C., McGraw-Herdeg, M., Cuesta, J., Aubry, A., Thorncroft, C., 2014. Synoptic scale dust emissions over the Sahara Desert initiated by a moist convective cold pool in early August 2006. *Q. J. R. Meteorol. Soc.* 140 <https://doi.org/10.1002/qj.2326>.
- Boucher, O., Randall, D., Artaxo, P., Bretherton, C., Feingold, G., Foster, P., Kerminen, V. M., Kondo, Y., Liao, H., Lohmann, U., et al., 2013. Clouds and Aerosols. In *Climate Change 2013: The Physical Science Basis. Contribution of Working Group I to the Fifth Assessment Report of the Intergovernmental Panel on Climate Change*. Cambridge University Press, Cambridge, UK; New York, NY, USA.
- Chaboureaud, J.-P., Bechtold, P., 2005. Statistical representation of clouds in a regional model and the impact on the diurnal cycle of convection during Tropical Convection, Cirrus and Nitrogen Oxides (TROCCINOX). *J. Geophys. Res.* 110, D17103.
- Chaboureaud, J.-P., Richard, E., Pinty, J.-P., Flamant, C., Di Girolamo, P., Kiemle, C., Behrendt, A., Chepfer, H., Chiriaco, M., Wulfmeyer, V., 2011. Long-range transport of Saharan dust and its radiative impact on precipitation forecast over Western Europe: a case study during the Convective and Orographically induced Precipitation Study (COPS). *Q. J. R. Meteorol. Soc.* 137, 236–251.
- Chaboureaud, J.-P., Flamant, C., Dauhut, T., Kocha, C., Lafore, J.P., Lavaysse, C., Marnas, F., Mokhtari, M., Pelon, J., Martínez, I.R., et al., 2016. Fenice dust forecast intercomparison over the Sahara in June 2011. *Atmos. Chem. Phys.* 16, 6977–6995.
- Chen, S., Kuo, Y., Ming, W., Ying, H., 1994. The effect of dust radiative heating on low-level frontogenesis. *J. Atmos. Sci.* 52, 1414–1420.
- Chen, D., Liu, Z., Davis, C., Gu, Y., 2017. Dust radiative effects on atmospheric thermodynamics and tropical cyclogenesis over the Atlantic Ocean using WRF-Chem coupled with an AOD Data Assimilation System. *Atmos. Chem. Phys.* 17, 7917–7939. <https://doi.org/10.5194/acp-177917-2017> (2017).
- Clerbaux, C., Boynard, A., Clarisse, L., George, M., Hadji-Lazaro, J., Herbin, H., Hurtmans, D., Pommier, M., Razavi, A., Turquety, S., Wespes, C., Coheur, P.-F., 2009. Monitoring of atmospheric composition using the thermal infrared IASI/MetOp sounder. *Atmos. Chem. Phys.* 9, 6041–6054.
- Crosman, E.T., Horel, J.D., 2010. Sea and lake breezes: a review of numerical studies. *Bound.-Layer Meteorol.* 137, 1–29. <https://doi.org/10.1007/s10546-010-9517-9>.
- Cuesta, J., Marsham, J.H., Parker, D.J., Flamant, C., 2009. Dynamical mechanisms controlling the vertical redistribution of dust and the thermodynamic structure of the West Saharan atmospheric boundary layer during summer. *Atmos. Sci. Lett.* 10, 34–42.
- Cuesta, J., Eremenko, M., Flamant, C., Dufour, G., Laurent, B., Bergametti, G., Höpfner, M., Orphal, J., Zhou, D., 2015. Three-dimensional distribution of a major desert dust outbreak over East Asia in March 2008 derived from IASI satellite observations. *J. Geophys. Res.-Atmos.* 120, 7099–7127. <https://doi.org/10.1002/2014JD022406> (2015).
- Cuesta, J., Flamant, C., Gaetani, M., Knippertz, P., Fink, A.H., Chazette, P., Eremenko, M., Dufour, G., Di Biagio, C., Formenti, P., 2020. Three-dimensional pathways of dust over the Sahara during summertime 2011 as revealed by new IASI observations. *Q. J. R. Meteorol. Soc.* <https://doi.org/10.1002/qj.3814>. Accepted Author Manuscript.
- Cuxart, J., Bougeault, P., Redelsperger, J.L., 2000. A turbulence scheme allowing for mesoscale and large-eddy simulations. *Q. J. R. Meteorol. Soc.* 126, 1–30.
- Dubovik, O., Sinyuk, A., Lapyonok, T., Holben, B.N., Mishchenko, M., Yang, P., Eck, T.F., Volten, H., Muñoz, O., Veihelmann, B., van der Zande, W.J., Leon, J.-F., Sorokin, M., Slutsker, I., 2006. Application of spheroidal models to account for aerosol particle nonsphericity in remote sensing of desert dust. *J. Geophys. Res.* 111, D11208. <https://doi.org/10.1029/2005JD006619>.
- Dumka, U.C., Kaskaoutis, D.G., Francis, D., Chaboureaud, J.-P., Rashki, A., Tiwari, S., et al., 2019. The role of the Intertropical Discontinuity region and the heat low in dust emission and transport over the Thar desert, India: a premonsoon case study. *J. Geophys. Res.-Atmos.* 124, 13197–13219. <https://doi.org/10.1029/2019JD030836>.
- Eager, R.E., Raman, S., Wooten, A., Westphal, D., Reid, J., Mandoos, A., 2008. A climatological study of the sea and land breezes in the Arabian Gulf region. *J. Geophys. Res.* 113 <https://doi.org/10.1029/2007JD009710>. D15106.
- Fiedler, S., Schepanski, K., Heinold, B., Knippertz, P., Tegen, I., 2014. How important are atmospheric depressions and mobile cyclones for emitting mineral dust aerosol in North Africa? *Atmos. Chem. Phys.* 14, 8983–9000.
- Francis, D., Eyras, C., Chaboureaud, J.-P., Mote, T., Holland, D., 2018. Polar jet associated circulation triggered a Saharan cyclone and derived the poleward transport of the African dust generated by the cyclone. *J. Geophys. Res.* <https://doi.org/10.1029/2018JD029095>.
- Francis, D., Eyras, C., Chaboureaud, J.-P., Mote, T., Holland, D., 2019a. A meandering polar jet caused the development of a Saharan cyclone and the transport of dust toward Greenland. *Adv. Sci. Res.* 1, 1–8. <https://doi.org/10.5194/asr-16-49-2019> (2019).
- Francis, D., Alshamsi, N., Cuesta, J., Isik, A.G., Dundar, C., 2019c. Cyclogenesis and density currents in the Middle East and the associated dust activity in September 2015. *Geosciences* 2019 (9), 376.
- Ge, C., Wang, J., Reid, J.S., 2014. Mesoscale modeling of smoke transport over the Southeast Asian Maritime Continent: couple of smoke direct radiative feedbacks below and above the low-level clouds. *Atmos. Chem. Phys.* 14, 159–174. <https://doi.org/10.5194/acp-14-159-2014>.
- Giannakopoulou, E.M., Toumi, R., 2012. The Persian Gulf summertime low-level jet over sloping terrain. *Q. J. R. Meteorol. Soc.* 138 (662), 145–157.
- Goudie, A.S., 2014. Desert dust and human health disorders. *Environ. Int.* 63, 101–113.
- Grimi, A., Tulet, P., Gomes, L., 2006. Dusty weather forecasts using the Meso-NH mesoscale atmospheric model. *J. Geophys. Res.* 111, D19205.
- Guiou, C., Al Azhar, M., Aumont, O., Mahowald, N., Levy, M., Ethé, C., Lachkar, Z., 2019. Major impact of dust deposition on the productivity of the Arabian Sea. *Geophys. Res. Lett.* 46, 6736–6744. <https://doi.org/10.1029/2019GL082770>.
- Haywood, J.M., Allan, R.P., Culverwell, I., Slingo, T., Milton, S., Edwards, J., Clerbaux, N., 2005. Can desert dust explain the outgoing longwave radiation anomaly over the Sahara during July 2003? *J. Geophys. Res.* 110, D05105. <https://doi.org/10.1029/2004JD005232>.
- Heald, C.L., Ridley, D.A., Kroll, J.H., Barrett, S.R.H., Cady-Pereira, K.E., Alvarado, M.J., Holmes, C.D., 2014. Contrasting the direct radiative effect and direct radiative forcing of aerosols. *Atmos. Chem. Phys.* 14, 5513–5527. <https://doi.org/10.5194/acp-14-5513-2014>.
- Heinold, B., Tegen, I., Schepanski, K., Hellmuth, O., 2008. Dust Radiative Feedback on Saharan Boundary Layer Dynamics and Dust Mobilization. *Geophys. Res. Lett.* 35, L20817. <https://doi.org/10.1029/2008GL035319>.
- Hermida, L., Merino, A., Sánchez, J.L., Fernández-González, S., García-Ortega, E., López, L., 2018. Characterization of synoptic patterns causing dust outbreaks that

- affect the Arabian Peninsula. *Atmos. Res.* 199 (2018), 29–39. ISSN 0169-8095. <https://doi.org/10.1016/j.atmosres.2017.09.004>.
- Hersbach, H., Bell, B., Berrisford, et al., 2020. The ERA5 global reanalysis. *Q. J. R. Meteorol. Soc.* <https://doi.org/10.1002/qj.3803>.
- IPCC, 2013. In: Stocker, T.F., Qin, D., Plattner, G.-K., Tignor, M., Allen, S.K., Boschung, J., Midgley, P.M. (Eds.), *Climate Change 2013: The Physical Science Basis. Contribution of Working Group I to the Fifth Assessment Report of the Intergovernmental Panel on Climate Change*. Cambridge University Press, Cambridge, United Kingdom and New York, NY, USA, 1535 pp.
- Jia, R., Liu, Y., Hua, S., Zhu, Q., Shao, T., 2018. Estimation of the aerosol radiative effect over the Tibetan Plateau based on the latest CALIPSO product. *J. Meteorol. Res.* 32, 707–722. <https://doi.org/10.1007/s13351-018-8060-3>.
- Jin, Q., Wei, J., Yang, Z.-L., Pu, B., Huang, J., 2015. Consistent response of Indian summer monsoon to Middle East dust in observations and simulations. *Atmos. Chem. Phys.* 15, 9897–9915. <https://doi.org/10.5194/acp-15-9897-2015>.
- Karagulian, F., Temimi, M., Ghebreyesus, D., et al., 2019. Analysis of a severe dust storm and its impact on air quality conditions using WRF-Chem modeling, satellite imagery, and ground observations. *Air Qual. Atmos. Health* 12, 453–470. <https://doi.org/10.1007/s11869-019-00674-z>.
- Karydis, V.A., Kumar, P., Barahona, D., Sokolik, I.N., Nenes, A., 2011. On the effect of dust particles on global cloud condensation nuclei and cloud droplet number. *J. Geophys. Res.* 116, D23204 <https://doi.org/10.1029/2011JD016283>.
- Kaskaoutis, D.G., Rashki, A., Housos, E.E., et al., 2015. Meteorological aspects associated with dust storms in the Sistan region, southeastern Iran. *Clim. Dyn.* 45, 407–424. <https://doi.org/10.1007/s00382-014-2208-3>.
- Kaskaoutis, D.G., Dumka, U.C., Rashki, A., Psiloglou, B.E., Gavriil, A., Mofidi, A., Petrino, K., Karagiannis, D., Kambezidis, H.D., 2019a. Analysis of intense dust storms over the eastern Mediterranean in March 2018: Impact on radiative forcing and Athens air quality. *Atmos. Environ.* 2019 (209), 23–39.
- Kaskaoutis, D.G., Francis, D., Rashki, A., Chaboureaud, J.-P., Dumka, U.C., 2019b. Atmospheric dynamics from synoptic to local scale during an intense frontal dust storm over the Sistan Basin in Winter 2019. *Geosciences* 2019 (9), 453.
- Kaufman, Y.J., Tanré, D., Rmer, L.A., Vermote, E.F., Chu, A., Holben, B.N., 1997. Operational remote sensing of tropospheric aerosol over land from EOS moderate resolution imaging spectroradiometer. *J. Geophys. Res.* 102 <https://doi.org/10.1029/96JD03988> (17,501-17,067).
- Kinne, S., Lohmann, U., Feichter, J., Schulz, M., Timmreck, C., Ghan, S., Easter, R., Chin, M., Ginoux, P., Takemura, T., Tegen, I., Koch, D., Herzog, M., Penner, J., Pitari, G., Holben, B., Eck, T., Smirnov, A., Dubovik, O., Slutsker, I., Tanre, D., Torres, O., Mishchenko, M., Geogdzhayev, I., Chu, D.A., Kaufman, Y., 2003. Monthly averages of aerosol properties: a global comparison among models, satellite data, and AERONET ground data. *J. Geophys. Res.-Atmos.* 108, 4634. <https://doi.org/10.1029/2001JD001253>.
- Kok, J.F., Ward, D.S., Mahowald, N.M., Evan, A.T., 2018. Global and regional importance of the direct dust-climate feedback. *Nat. Commun.* 9 (241), 1–11.
- Kosmopoulos, P.G., Kazadzis, S., Taylor, M., Athanasopoulou, E., Speyer, O., Raptis, P.I., Marinou, E., Proestakis, E., Solomos, S., Gerasopoulos, E., Amiridis, V., Bais, A., Kontos, C., 2017. Dust impact on surface solar irradiance assessed with model simulations, satellite observations and ground-based measurements. *Atmos. Meas. Tech.* 10, 2435–2453. <https://doi.org/10.5194/amt10-2435-2017>.
- Krishnamurti, T.N., Stefanova, L., Misra, V., 2013. *Tropical Meteorology: An Introduction*, 4th ed. Springer. <https://doi.org/10.1007/978-1-4614-7409-8>. 423 pp.
- Lac, C., Chaboureaud, J.-P., Masson, V., Pinty, P., Tulet, P., Escobar, J., Leriche, M., Barthe, C., Aouizerats, B., Augros, C., et al., 2018. Overview of the Meso-NH model version 5.4 and its applications. *Geosci. Model Dev.* 11, 1929–1969.
- Lafore, J.P., Stein, N., Asencio, J., Bougeault, P., Ducrocq, V., Duron, J., Fischer, C., Hereil, P., Mascart, P., Pinty, J.P., et al., 1998. The Meso-NH Atmospheric simulation System. Part I: adiabatic formulation and control simulations. *Scientific objectives and experimental design*. *Ann. Geophys.* 16, 90–109.
- Lavaysse, C., Chaboureaud, J.-P., Flamant, C., 2011. Dust impact on the West African heat low in summertime. *Q.J.R. Meteorol. Soc.* 137, 1227–1240. <https://doi.org/10.1002/qj.844>.
- Lemaitre, C., Flamant, C., Cuesta, J., Raut, J.-C., Chazette, P., Formenti, P., Pelon, J., 2010. Radiative heating rates profiles associated with a spring time case of Bodele and Sudan dust transport over West Africa. *Atmos. Chem. Phys.* 10, 8131–8150. DOI: 10.8131-8150.
- Liu, Y., Jia, R., Dai, T., Xie, Y., Shi, G., 2014. A review of aerosol optical properties and radiative effects. *J. Meteorol. Res.* 28, 1003–1028. <https://doi.org/10.1007/s13351-014-4045-z>.
- Maghrabi, A.H., Al-Dosari, A.F., 2016. Effects on surface meteorological parameters and radiation levels of a heavy dust storm occurred in Central Arabian Peninsula. *Atmos. Res.* 182 (2016), 30–35. ISSN 0169-8095. <https://doi.org/10.1016/j.atmosres.2016.07.024>.
- Mallet, M., Tulet, P., Serça, D., Solmon, F., Dubovik, O., Pelon, J., Pont, V., Thouroun, O., 2009. Impact of dust aerosols on the radiative budget, surface heat fluxes, heating rate profiles and convective activity over West Africa during March 2006. *Atmos. Chem. Phys.* 9, 7143–7160. <https://doi.org/10.5194/acp-9-7143-2009>.
- Mashat, A.S., Alamodi, A.O., Ahmed, H.A.M., 2008. *Diagnostic and Prognostic Study for Dust (Sand) Storms over Saudi Arabia*. Tech. Rep. V18 AR-26–89. King Abdulaziz University, Faculty of Meteorology, Environment and Arid Land Agriculture, Saudi Arabia.
- Middleton, N.J., Kang, U., 2017. Sand and dust storms: impact mitigation. *Sustainability* 9, 1053.
- Mlawer, E.J., Taubman, S.J., Brown, P.D., Iacono, M.J., Clough, S.A., 1997. Radiative transfer for inhomogeneous atmospheres: RRTM, a validated correlated-k model for the longwave. *J. Geophys. Res.* 102D, 16663–16682.
- Myhre, G., Shindell, D., Breon, F.-M., Collins, W., Fuglestad, J., Huang, J., Koch, D., Lamarque, J.-F., Lee, D., Mendoza, B., Nakajima, T., Robock, A., Stephens, G., Takemura, T., Zhang, H., 2013. Anthropogenic and natural radiative forcing. In: Stocker, T.F., Qin, D., Plattner, G.-K., Tignor, M., Allen, S.K., Boschung, J., Midgley, P.M. (Eds.), *Climate Change 2013: The Physical Science Basis. Contribution of Working Group I to the Fifth Assessment Report of the Intergovernmental Panel on Climate Change*. Cambridge University Press, Cambridge, United Kingdom and New York, NY, USA.
- Nelli, N.R., Temimi, M., Fonseca, R.M., Weston, M.J., Thota, M.S., Valappil, V.K., Branch, O., Wulfmeyer, V., Wehbe, Y., Al Hosary, T., Shalaby, A., Al Shamsi, N., Al Naqbi, H., 2020. Impact of roughness length on WRF simulated Land-Atmosphere interactions over a hyper-arid region. *J. Earth Space Sci.* 7 <https://doi.org/10.1029/2020EA001165> e2020EA001165.
- Notaro, M., Yu, Y., Kalashnikova, O.V., 2015. Regime shift in Arabian dust activity, triggered by persistent Fertile Crescent drought. *J. Geophys. Res. Atmos.* 120, 10,229–10,249. <https://doi.org/10.1002/2015JD023855>.
- Pinty, J.-P., Jabouille, P., 1998. A mixed-phase cloud parameterization for use in a mesoscale non-hydrostatic model: Simulations of a squall line and of orographic precipitations. In: *Conference on Cloud Physics*. American Meteorological Society, Everett, WA, USA, pp. 217–220.
- Prakash, P.J., Stenchkov, G., Kalenderski, S., Osipov, S., Bangalath, H., 2015. The impact of dust storms on the Arabian Peninsula and the Red Sea. *Atmos. Chem. Phys.* 15, 199–222. <https://doi.org/10.5194/acp-15-199-2015>.
- Prospero, J.M., Ginoux, P., Torres, O., Nicholson, S.E., Gill, T.E., 2002. Environmental characterization of global sources of atmospheric soil dust identified with the NIMBUS 7 Total ozone mapping spectrometer (TOMS) absorbing aerosol product. *Rev. Geophys.* 40 (1), 1002. <https://doi.org/10.1029/2000RG000095>.
- Rao, P.G., Al-Sulaiti, M., Al-Mulla, A.H., 2001. Winter Shamals in Qatar, Arabian Gulf. *Weather* 56, 444–451 (b).
- Rap, A., Scott, C.E., Spracklen, D.V., Bellouin, N., Forster, P.M., Carslaw, K.S., Schmidt, A., Mann, G., 2013. Natural aerosol direct and indirect radiative effects. *Geophys. Res. Lett.* 40, 3297–3301. <https://doi.org/10.1002/grl.50441>.
- Rashki, A., Kaskaoutis, D.G., Mofidi, A., Minvielle, F., Chiapello, I., Legrand, M., Dumka, U.C., Francois, P., 2019. Effects of Monsoon, Shamal and Levant winds on dust accumulation over the Arabian Sea during summer – the July 2016 case. *Aeolian Res.* 36, 27–44.
- Saeed, T.M., Al-Dashti, H., Spyrou, C., 2014. Aerosol's optical and physical characteristics and direct radiative forcing during a shamal dust storm, a case study. *Atmos. Chem. Phys.* 14, 3751–3769. <https://doi.org/10.5194/acp-14-3751-2014> (2014).
- Saeedi, A., Khoshakhlagh, F., 2019. A composite analysis of the morning cyclone in two Asian deserts. *Theor. Appl. Climatol.* 137, 713–727. <https://doi.org/10.1007/s00704-018-2607-1>.
- Saleeby, S.M., van den Heever, S.C., Bukowski, J., Walker, A.L., Solbrig, J.E., Atwood, S.A., Bian, Q., Kreidenweis, S.M., Wang, Y., Wang, J., Miller, S.D., 2019. The influence of simulated surface dust lofting and atmospheric loading on radiative forcing. *Atmos. Chem. Phys.* 19, 10279–10301. <https://doi.org/10.5194/acp-19-10279-2019>.
- Schepanski, K., 2018. Transport of mineral dust and its impact on climate. *Geosciences* 8, 151. <https://doi.org/10.3390/geosciences8050151>.
- Sharma, D., Singh, D., Kaskaoutis, D.G., 2012. Impact of two intense dust storms on aerosol characteristics and radiative forcing over Patiala, Northwestern India. *Adv. Meteorol.* 2012 <https://doi.org/10.1155/2012/956814>. Article ID 956814, 13 pages.
- Slingo, A., Ackerman, T.P., Allan, R.P., Kassianov, E.I., McFarlane, S.A., Robinson, G.J., Barnard, J.C., Miller, M.A., Harries, J.E., Russell, J.E., Dewitte, S., 2006. Observations of the impact of a major Saharan dust storm on the atmospheric radiation balance. *Geophys. Res. Lett.* 33, L24817. <https://doi.org/10.1029/2006GL027869>.
- Sokolik, I.N., Toon, O.B., 1996. Direct radiative forcing by anthropogenic airborne mineral aerosols. *Nature* 381, 681–683. <https://doi.org/10.1038/381681a0>.
- Spyrou, C., 2018. Direct radiative impacts of desert dust on atmospheric water content. *Aerosol Sci. Technol.* 52 (6), 693–701. <https://doi.org/10.1080/02786826.2018.1449940>.
- Stephens, G.L., Vane, D.G., Boain, R.J., Mace, G.G., Sassen, K., Wang, Z., Illingworth, A.J., O'Connor, E.J., Rossow, W.B., Durden, S.L., Miller, S.D., Austin, R.T., Benedetti, A., Mitrescu, C., 2002. The CloudSat mission and the A-Train. *Bull. Am. Meteorol. Soc.* 83, 1771–1790.
- Tanaka, T.Y., Chiba, M., 2006. A numerical study of the contributions of dust source regions to the global dust budget. *Glob. Planet. Chang.* 52, 88–104. <https://doi.org/10.1016/j.gloplacha.2006.02.002>.
- Tegen, I., Lacis, A.A., 1996. Modeling of particle size distribution and its influence on the radiative properties of mineral dust aerosol. *J. Geophys. Res.* 101, 19237–19244. <https://doi.org/10.1029/95JD03610> (1996).
- Todd, M.C., Bou Karam, D., Cavazos, C., Bouet, C., Heinold, B., Baldasano, J.M., Cautenet, G., Koren, I., Perez, C., Solmon, F., Tegen, I., Tulet, P., Washington, R., Zakey, A., 2008. Quantifying uncertainty in estimates of mineral dust flux: an inter-comparison of model performance over the Bédélé Depression, Northern Chad. *J. Geophys. Res.* 113, D24107. <https://doi.org/10.1029/2008JD010476>.
- Tulet, P., Crassier, V., Cousin, F., Shure, K., Rosset, R., 2005. ORILAM, a three moment lognormal aerosol scheme for mesoscale atmospheric model. On-line coupling into the Meso-NH-C model and validation on the Escompte campaign. *J. Geophys. Res.* 110, D18201.

- Tulet, P., Mallet, M., Pont, V., Pelon, J., Boone, A., 2008. The 7–13 March 2006 dust storm over West Africa: generation, transport, and vertical stratification. *J. Geophys. Res.* 113, D00C08. <https://doi.org/10.1029/2008JD009871>.
- Wang, J., Nair, U., Christopher, S.A., 2004. GOES-8 Aerosol optical thickness assimilation in a mesoscale model: Online integration of aerosol radiative effects. *J. Geophys. Res.* 109 <https://doi.org/10.1029/2004JD004827>. D23203.
- Wang, W., Huang, J., Zhou, T., Bi, J., Lin, L., Chen, Y., Huang, Z., Su, J., 2013a. Estimation of radiative effect of a heavy dust storm over Northwest China using Fu–Liou model and ground measurements. *Elsevier J. Quant. Spectr. Radiat. Transf.* 122, 114–126. <https://doi.org/10.1016/j.jqsrt.2012.10.018>. June 2013.
- Wang, H., Shi, G.-Y., Zhu, J., Chen, B., Che, H., Zhao, T., 2013b. Case study of longwave contribution to dust radiative effects over East Asia. *Chin. Sci. Bull.* 58, 3673–3681. <https://doi.org/10.1007/s11434-013-5752-z>.
- Weston, M.J., Temimi, M., Nelli, N.R., Fonseca, R.M., Thota, M.S., Valappil, V.K., 2020. On the analysis of the low-level double Temperature inversion over the United Arab Emirates: A case study during april 2019. In: *IEEE Geoscience and Remote Sensing Letters*. <https://doi.org/10.1109/LGRS.2020.2972597>.
- Wielicki, B.A., Barkstrom, B.R., Harrison, E.F., Lee, R.B., Smith, G.L., Cooper, J.E., 1996. Clouds and the Earth's Radiant Energy System (CERES): an earth observing system experiment. *Bull. Amer. Meteor. Soc.* 77, 853–868. [https://doi.org/10.1175/1520-0477\(1996\)077<0853:CATERE>2.0.CO;2](https://doi.org/10.1175/1520-0477(1996)077<0853:CATERE>2.0.CO;2).
- Yang, Y., Russell, L.M., Lou, S., Liao, H., Guo, J., Liu, Y., Singh, B., Ghan, S.J., 2017. Dust-wind interactions can intensify aerosol pollution over eastern China. *Nat. Commun.* 8, 15333. <https://doi.org/10.1038/ncomms15333>.
- Yu, Y., Notaro, M., Liu, Z., Wang, F., Alkolibi, F., Fadda, E., Bakhrjy, F., 2015. Climatic controls on the interannual to decadal variability in Saudi Arabian dust activity: toward the development of a seasonal dust prediction model. *J. Geophys. Res. Atmos.* 120, 1739–1758. <https://doi.org/10.1002/2014JD022611>.
- Yu, Y., Notaro, M., Kalashnikova, O.V., Garay, M.J., 2016. Climatology of summer Shamal wind in the Middle East. *J. Geophys. Res. Atmos.* 121, 289–305. <https://doi.org/10.1002/2015JD024063>.
- Zender, C.S., Bian, H.S., Newman, D., 2003. Mineral Dust Entrainment and Deposition (DEAD) model: description and 1990s dust climatology. *J. Geophys. Res.* 108, 4416.
- Zhao, C., Liu, X., Ruby Leung, L., Hagos, S., 2011. Radiative impact of mineral dust on monsoon precipitation variability over West Africa. *Atmos. Chem. Phys.* 11 (1879–1893), 2011. <https://doi.org/10.5194/acp-11-1879-2011>.